Hydroxymethylated-*P16* Allele Is Transcription-Inactive

Ying Gan[#], Paiyun Li[#], Xiao Han[#], Sisi Qin, Chenghua Cui, Zhaojun Liu, Jing Zhou, Liankun Gu, Zhe-ming Lu, Baozhen Zhang*, Dajun Deng*

Key Laboratory of Carcinogenesis and Translational Research (Ministry of Education/ Beijing), Division of Etiology, Peking University Cancer Hospital and Institute, Fu-Cheng-Lu #52, Haidian District, Beijing, 100142, China

[#] Equal contribution

* Corresponding authors

Author contributions

YG and PL: elucidated the biological function of *P16* hydroxymethylation; SQ: discovered *P16* hydroxymethylation and its association with gastric carcinogenesis; XH: demonstrated the strand-bias distribution of 5hmCs in the *P16* alleles; CC, Z-mL, and BZ: constructed the *P16*-specific oxygenase; LG performed the animal experiments; BZ performed immunostaining and cell sorting assays and codesigned the study; ZL and JZ: carried out other experiments; DD: designed the study, analyzed the data, and wrote the manuscript. All authors read and approved the final manuscript.

Running title: DNA hydroxymethylation does not reactivate gene transcription

ABSTRACT

Background: 5-Methylcytosine can be oxidized into 5-hydroxymethylcytosine (5hmC) in the genome. Methylated-*P16* (P16M) can be oxidized into completely hydroxymethylated-*P16* (P16H) in human cancer and precancer cells. The aim of this study is to investigate the biological function of P16H.

Methods: True P16M and P16H were analyzed using bisulfite/TAB-based assays. A ZFP-based *P16*-specific dioxygenase (P16-TET) was constructed and used to induce P16H. Cell proliferation and migration were determined with a series of biological analyses.

Results: (**A**) The 5hmCs were enriched in the antisense-strand of the *P16* exon-1 in HCT116 and AGS cells containing methylated-*P16* alleles (P16M). (**B**) P16-TET induced both P16H and *P16* demethylation in H1299 and AGS cells and reactivated *P16* expression. Notably, P16H was only detectable in the sorted P16-TET H1299 and AGS cells that did not show *P16* expression. (**C**) P16-TET significantly inhibited the xenograft growth derived from H1299 cells in NOD-SCID mice, but did not inhibit the growth of *P16*-deleted A549 control cells. *P16*-siRNA knockdown could rescue P16-TET-inhibited cell migration.

Conclusion: Hydroxymethylated *P16* alleles are transcriptionally inactive.

Key words: *P16* gene; CpG islands; methylation; hydroxymethylation; epigenetic editing

AUTHOR SUMMARY

It is well known that 5-methylcytosine (5mC) in genomic DNA of mammalian cells can be oxidized into 5-hydroxymethylcytosine (5hmC) and other derivates by DNA dioxygenase TETs. While conversion of 5mC to 5hmC plays an important role in active DNA demethylation through further oxidations, a certain proportion of 5hmCs remain in the genome. Although it is supposed that occurrence of 5hmCs may contribute to the flexibility of chromatin and the protection of the bivalent promoters from hypermethylation, the direct effect of 5hmCs on gene transcription is unknown. In the present study, we engineered a zinc-finger protein-based P16-specific DNA dioxygenase and used it to induce *P16* hydroxymethylation and demethylation in cancer cells. Our results demonstrate, for the first time, that the hydroxymethylated *P16* alleles retain transcriptionally inactive. This is supported by our recent findings that mRNAs are always transcribed only from the unmethylated P16 strands, but not from the hydroxymethylated/methylated strands in HCT116 cells, and that the risks for malignant transformation are similar for patients with the *P16* methylation-positive oral epithelial dysplasia with and without *P16* hydroxymethylation in a prospective study.

INTRODUCTION

It is well known that ten-eleven translocation methylcytosine dioxygenases (TET-1/2/3) oxidize 5-methylcytosine (5mC) to 5-hydroxymethylcytosine (5hmC), 5-formylcytosine (5fC), and 5-carboxylcytosine (5caC) in the genome [1-4]. While oxidation of 5mC leads to active DNA demethylation, a certain proportion of 5hmC sites remain in the genome with a strand-asymmetric and strand-symmetric distribution pattern that provides its own regulatory function [5-9]. Although it is frequently reported that the 5hmC level of some genes is positively correlated with increased gene expression, it is not clear whether 5hmC itself or related DNA demethylation contribute to the reactivation of gene transcription.

Typical bisulfite-based assays cannot discriminate 5mCs from 5hmCs. The classic term “DNA methylation” is, in fact, total DNA methylation, including true methylation and hydroxymethylation. Total methylation of the CpG island (CGI) flanking the transcription start site (TSS) in the *P16* gene (*CDKN2A*) is prevalent in human cancer and precancerous tissues [10,11] and is linked to increased cancer development from epithelial dysplasia in many organs [12-18]. *P16* methylation (P16M) not only directly inactivates *P16* transcription [19] but also represses *ANRIL* transcription [20]. Our recent study demonstrated that there were dense 5hmCs in the *P16* exon-1 CGI in HCT116 cells, and no mRNA transcripts from the hydroxymethylated *P16* (P16H) alleles were detected in the cells [21,22]. P16H was detected in 9.3% of human oral epithelial dysplasia (OED) tissues [23]. However, the malignant transformation risk was similar between P16M-positive OED patients with and without P16H. It is a fundamental question in epigenetic research to clarify whether hydroxymethylation of TSS-flanking CGIs leads to transcriptional activation of genes.

In this study, we characterized the distribution patterns of 5hmCs within the sense and

antisense strands (S- and AS-strands) of the *P16* promoter and exon-1 CGIs using detailed TET-assisted bisulfite (TAB)-based assays, and found that 5hmCs were enriched in the AS-strands of *P16* exon-1 CGIs in cancer cells. To elucidate the possible role of P16H, an epigenetic editing tool, *P16*-specific TET-1 (P16-TET), was constructed and used to induce P16H in cancer cell lines. Notably, our data showed, for the first time, that P16H itself could not reactivate gene transcription.

RESULTS

Characterization of 5hmCs in the *P16* Exon-1 CGI

We recently found that there were dense 5hmCs in the *P16* exon-1 in HCT116 cells [21], in which the wildtype *P16* alleles are silenced by DNA methylation and the mutant alleles containing a G-insertion in exon-1 are unmethylated. To characterize the distribution pattern of 5hmCs in the *P16* CGI, the S- and AS-strands of the *P16* promoter and the exon-1 regions were amplified using conventional bisulfite-modified and TAB-modified single-strand DNA samples from HCT116 cells as templates. Next, the proportions of total P16M- and P16H-containing fragments were quantitatively analyzed by denaturing high performance liquid chromatography (DHPLC). As expected, the total P16M peak and the P16U peak were both detected in the all bisulfite PCR products from both the S- and AS-strands of the *P16* promoter and exon-1 fragments (Figure 1A-D: HCT116, left charts). However, a high P16H peak was detected only in the exon-1 AS-strand and the P16H proportion reached up to 88% (=0.77/0.87) (Figure 1D: HCT116_TAB, left chart). In the promoter AS-strand fragment, the P16H peak was very low (Figure 1C: HCT116_TAB, left chart). In the S-strands of the promoter and exon-1 fragments, much lower levels of the P16H peaks were detected (Figures 1A and 1B: HCT116_TAB, left charts).

The TAB sequencing results for the HCT116_TAB PCR products confirmed the DHPLC analysis results (Figure 1A-D: right charts). Dense 5hmCs were found in the wildtype exon-1 AS-strand (tracked with a G-deletion; 5hmC-density, 82.9%), but not in the paired S-strand (5hmC-density, 17.6%). No clone containing more than one 5hmC was detected in the promoter AS-strand (5hmC density, 2.0%). Sporadic 5hmCs were distributed in the promoter S-strand (5hmC density, 22.3%). Together, the results of the TAB-DHPLC and TAB sequencing analyses consistently demonstrated that 5hmCs were enriched mainly in the AS-strand of the wild-type *P16* exon-1 in HCT116 cells. This indicates that wild-type *P16* exon-1 is hydroxymethylated mainly in the AS-strand and is methylated truly in the S-strand in HCT116 cells. As described below, dense 5hmC sites were also detected in the AS-strand of the *P16* exon-1 in gastric cancer AGS cells.

Construction of Engineered P16-TET

To study whether P16H affects gene transcription, an expression controllable *P16*-specific dioxygenase P16-TET and its inactive mutant control vector were constructed through fusing an engineered *P16* promoter-specific seven zinc finger protein (7ZFP-6I) [24] with the catalytic domain of human TET1 and integrated into the pcDNA3.1 expression vector (Figure S2A). H1299 cells were chosen because epigenetic editing of the methylated *P16* CGIs by the *P16*-specific transcription factor (P16-ATF; 7ZFP-6I-VP64) has been optimized in this cell type [24]. As expected, the results of both qRT-PCR and immunofluorescence staining showed that the methylated *P16* alleles were re-activated in H1299 cells 6 days after transient transfection with the P16-TET vector (Figure 2). Such *P16* reactivation was not observed in the P16-TET mutant control cells. This indicates that P16-TET is *P16* gene reactive and could be used in further studies.

Induction of P16H by P16-TET

To study the possible biological functions of *P16*-specific hydroxymethylation, the P16-TET coding sequence was further integrated into the pTRIPZ lentivirus vector carrying a "Tet-on" switch to allow the gene expression to be controlled for stable transfection (Figure S2B). In the P16-TET stably transfected H1299 cells, the results of the TAB methylation-specific PCR (MSP) analysis showed that P16H signals appeared in the P16-TET cells 3 days after the induction of doxycycline (Dox; final conc. 0.25 μg/mL) (P16-TET&Dox_3d; Figure 2A, TAB-MSP), but did not appear in cells transfected with the empty vector (control cells with Dox treatment) (Vector&Dox_14d) or in baseline P16-TET cells without Dox induction, in which only nonhydroxymethylated *P16* alleles (P16N) were detected. In the MSP analysis, P16U was detectable in the P16-TET&Dox cells 3 days following Dox induction (Figure 3A, MSP). The bisulfite-DHPLC results showed that a low P16U peak was detected beginning on the 14th day (Figure S3A, red-arrow). Two P16U clones were also observed on the 28th day from the bisulfite sequencing (Figure S3B, red-star). These results indicate that both P16H and P16U were induced in the P16-TET&Dox cells.

Furthermore, the Western blot results revealed that P16 protein was detected in the P16-TET&Dox cells since the 7th day, but not in the Vector&Dox control cells (7d; Figure 3B). The qRT-PCR results showed a weak reactivation of *P16* transcription beginning on the 4th day (Figure 3C). The immunofluorescence confocal microscopy results confirmed the presence of P16 protein in the nuclei of H1299 cells (Figure 3D). In addition, the expression status of the control genes *P15* and *P14* was not affected, whereas the expression level of *ANRIL,* which is coordinately expressed with *P16*, was increased

(Figure S4). This suggests a high specificity for the zinc finger protein-based P16-TET to induce P16H and P16U.

Similarly, on the 7th day after Dox induction, transcriptional reactivation of *P16* was also observed in P16-TET stably transfected gastric cancer AGS cells, in which *P16* alleles are homogenously methylated (Figures 4A-4E). Interestingly, P16U signals were not detected in P16-TET AGS cells after Dox induction for 11 days (P16-TET&Dox_11d) in the bisulfite-DHPLC and bisulfite sequencing analyses (Figure 4A and 4C). P16H signals were observed in the TAB-DHPLC and TAB sequencing results (Figure 4B and 4D), indicating that hydroxymethylation occurred earlier than demethylation at P16 CGIs. A few baseline 5hmCs were also found in the *P16* exon-1 AS-strand of AGS mock control cells. Although weak *P16* mRNA signals were detected in P16-TET AGS cells after Dox induction for 7 days and 11 days according to sensitive RT-PCR analysis (Figure 4E), P16 protein was not detected in these cells according to the insensitive Western blot analysis (Figure 4F).

Transcription Silencing of *P16* alleles by Hydroxymethylation

To clarify whether DNA hydroxymethylation or demethylation contributes to *P16* reactivation, we further analyzed the hydroxymethylation status of *P16* CGIs in cell subpopulations with strong, weak, and no P16 staining (P16(+), P16(±), and P16(-)) that were sorted from P16-TET&Dox_21d H1299 cells (Figure 5A). Interestingly, P16H signal was detected only in the P16(-) subpopulation, but not in the P16(+) and P16(±) subpopulations in the TAB-MSP analysis (Figure 5B). TAB sequencing also showed dense 5hmCs among 3 of the 14 clones (21.4%) of the exon-1 AS-strand TAB-PCR products from the P16(-) subpopulation, with an average hydroxymethylation density of 95.2% for these 3 clones (Figure 5C). The occurrence of 5hmCs in the promoter AS-strand was not detected

in the TAB-DHPLC and TAB sequencing results (data not shown).

The above results were further confirmed in AGS cells. As described above, P16 protein could not be detected in P16-TET&Dox AGS cells after Dox treatment for 11 days (Figure 4F). To obtain a P16(+) AGS subpopulation by FACS, the DNA methyltransferase inhibitor 5-aza-deoxycytidine (DAC, final concentration 20 nmol/L) was used to increase the P16 protein level within P16-TET AGS cells. In the immunostaining cell analysis, nucleic P16 protein was detected in 3.5% of P16-TET AGS cells after DAC treatment for 10 days (P16-TET&DAC_10d, with baseline P16-TET expression without Dox induction), while nucleic P16 protein was detected in only 0.5% of the AGS cells treated with DAC alone (Figure S5). Next, the P16(+), P16(±), and P16(-) subpopulations were sorted from these P16-TET&DAC_10d AGS cells (Figure 6A). Once again, the P16H signal was detected only in the P16(-) subpopulation, and not in the P16(+) and P16(±) cells by the TAB-MSP and TAB-DHPLC assays (Figures 6B and 6C). In contrast, P16N signal was detected in all three subpopulations. The TAB sequencing results confirmed this. Dense 5hmCs were observed in the *P16* exon-1 AS-strand in the P16(-) subpopulation, but not in the P16(+) subpopulation (Figure 6E).

Collectively, the above results indicate that P16H occurs only in P16(-) cells, and not in P16(+) and P16(±) cells, suggesting that the P16H alleles should be transcriptionally inactive.

***P16* Allele-Dependent Inhibition of Tumor Growth by P16-TET**

Although a proliferation difference was not observed between the P16-TET and control vector, which were stably transfected in H1299 cells *in vitro* (Figure 7A), the average weight of tumor xenograftsof the P16-TET stably transfected cells was significantly lower than that

of the control cells in NOD-SCID mice (*n*=8) on the 50th post-transplantation day (*P*<0.001, Figures 7B and 7C). Morphologic differences were not observed between P16-TET and control vector xenografts (Figure 7D). This result was confirmed in a repeat experiment (Figure S6A). Meanwhile, this difference could not be observed in xenograft tumors from lung cancer A549 control cells in which the *P16-P15-P14* alleles were homogeneously deleted (Figure S6B). These data suggest that P16-TET may specifically inhibit the growth of cancer cells *in vivo* in a *P16* allele-dependent manner.

Although P16-TET did not affect the proliferation of H1299 cells *in vitro*, the results of the IncuCyte ZOOM wound-scratch and typical transwell assays showed that P16-TET significantly inhibited H1299 cell migration (Figures S7A and S7B). In a rescue assay, *P16* siRNA-knockdown significantly reversed the inhibited migration of the P16-TET&Dox H1299 cells (Figure S7C). These results provide further evidence to support that P16-TET may inhibit cell migration through *P16* reactivation.

DISCUSSION

DNA hydroxymethylomes at the base-resolution level have been analyzed in embryonic stem cells, adult tissues, and tumors [25-31]. Many functions of DNA hydroxymethylation in the genome have been illustrated by *TET-1/2/3* knockout studies [5-7,27,31,32]. However, the actual effect of hydroxymethylation of CGIs on gene transcription remains elusive. In the present study, we demonstrated that 5hmCs were enriched in the AS-strand of the *P16* exon-1 CGI. Most importantly, this study showed for the first time that DNA hydroxymethylation itself could not reactivate *P16* gene transcription. Instead, hydroxymethylation-mediated active DNA demethylation could reactivate *P16* gene transcription, which subsequently inhibited the migration and growth of cancer cells *in vivo*.

It is well known that an appropriate proportion of 5hmCs in the genome is distributed with a strand bias [9,28]. We recently reported that there were dense 5hmCs in the *P16* exon-1 AS-strands in HCT116 cells [21,22]. Based on the comprehensive TAB-DHPLC and TAB sequencing results, here, we further demonstrated that 5hmCs were enriched only in the AS-strand of the *P16* exon-1 in HCT116 cells and AGS cells, while sporadic 5hmCs were detected in the S-strand of *P16* promoter and exon-1 regions. The fact that 88% of the exon-1 AS-strand CpGs in the wild-type *P16* alleles in HCT116 cells are hydroxymethylated indicates that *P16* exon-1 has a methylation: hydroxymethylation (M:H) mixture, composed of a fully hydroxymethylated AS-strand and a truly methylated S-strand.

It has been reported that triple knockout of *TET-1/2/3* led to bivalent promoter hypermethylation in H1 cells [33]. TSSs are DNA replication start sites. S- and AS-strands of genes are generally replicated by different types of DNA polymerases in eukaryotic cells (Polδ for the leading strand and Polα for the lagging strand). Unlike true DNA methylation that is maintained by DNMT1 during DNA synthesis in the S-phase of the cell cycle, DNA hydroxymethylations are probably maintained by the *de novo* methyltransferases DNMT3a/b [34]. It is of great interest to study the mechanisms leading to the strand bias of DNA hydroxymethylation.

Three types of epigenetic editing methods, including ZFP-, transcription activator-like effector (TALE)-, and CRISPR/dCas9-based systems, have emerged as advanced tools to study the functions of epigenetic modifications [19,35-39]. According to the reported data, the specificity and efficiency of ZFP-based epigenetic editing tools are likely higher than those of TALE-based editing tools or CRISPR/dCas9-based editing tools. For example, the expression controllable ZFP-based P16-Dnmt could selectively methylate entire *P16* CGIs

238 around the TSS [19]. However, CRISPR/dCas9-Dnmt3a, combined with *P16*-sgRNA, could
239 specifically methylate only approximately 50 bp sgRNA target-flanking sequences (not
240 including the sgRNA target) [40,41]. In contrast, *P16* TALE-Dnmt could methylate the *P16*
241 target and other CGIs within the *P15-P14-P16-MTAP* gene cluster and repress their
242 transcription, with low specificity [42]. We recently reported that *ANRIL* expression was
243 repressed in cancer cells by *P16* methylation [20]. Here, we further demonstrated that the
244 *ANRIL* expression was upregulated in the P16-TET-expressing cells and that the mRNA
245 levels of *P15* and *P14* were not increased. These observations suggest that P16-TET could
246 specifically demethylate *P16* CGIs via DNA hydroxymethylation and reactivate the
247 transcription of both the *P16* and *ANRIL* genes, though DNA hydroxymethylation itself
248 could not reactivate *P16* gene transcription.

249 Recently, we found that all *P16* mRNA clones in the HCT116 cells were transcribed
250 only from the unmethylated *P16* alleles, and none from the methylated: hydroxymethylated
251 (M:H) *P16* alleles [21], and that both true P16M and P16H could similarly increase the risk
252 for malignant transformation of oral epithelial dysplasia in a prospective study [23]. The
253 findings of the present study show that the P16-TET-induced hydroxymethylation of *P16*
254 alleles in both H1299 and AGS cells retain transcriptional silence, which provides a
255 possible mechanism to explain the above observations.

256 There are many differences between cell culture and animal models. Although the
257 proliferation of H1299 cells that are stably transfected with P16-TET was not changed
258 under *in vitro* culture conditions, the growth of xenograft tumors from these cells was
259 obviously inhibited in host mice. The exact reasons leading to this difference are unknown;
260 however, the reactivation of methylated *P16* alleles via DNA demethylation by P16-TET

may account for the growth inhibition *in vivo*. The growth inhibition of xenograft tumors from the *P16*-deleted A549 control cells was not observed, suggesting that the growth inhibition of xenografts by P16-TET may be a *P16*-dependent phenomenon. In the rescue assay, siRNA knockdown of P16-TET-reactivated *P16* expression almost completely reversed the inhibition of P16-TET-induced cell migration. This further suggests that the inhibition of the cancer cell migration by P16-TET may be a *P16*-specific effect.

In conclusion, we found that hydroxymethylation of *P16* CGI is located mainly in the exon-1 AS-strand. P16H alleles are transcriptionally inactive. *P16* demethylation via hydroxymethylation could reactivate gene transcription and inhibit the growth of cancer cells.

METHODS

Cell Lines and Culture

The colon cancer cell line HCT116 was purchased from the American Type Culture Collection (ATCC). The GC cell line AGS and the lung cancer cell line H1299 were kindly provided by Prof. Chengchao Shou from the Peking University Cancer Hospital and Institute. The colon cancer cell line, RKO was kindly provided by Prof. Guoren Deng from the University of California, San Francisco. These cells were cultured in RPMI 1640 containing 10% FBS and 100 U/mL penicillin/streptomycin (Invitrogen, California, USA) at 37°C in a humidified incubator with 5% CO_2.

These cell lines were tested and authenticated by Beijing JianLian Genes Technology Co., LTD before they were used in this study. STR patterns were analyzed using a Goldeneye^{TM}20A STR Identifiler PCR Amplification Kit. Gene Mapper v3.2 software (ABI)

was used to match the STR pattern with the ATCC online databases.

Characterization of 5mC and 5hmC Sites in *P16* CGIs

Total P16M was analyzed using 150-bp regular methylation-specific PCR (MSP) [43]. To selectively detect P16H, the genomic DNA (3 μg), spiked with *M.sss*I-methylated and 5hmC-containing λ-DNA controls, was modified using the TET-Assisted Bisulfite (TAB) Kit, according to manufacturer's instructions (WiseGene, Cat# K001). During TAB-modification, 5mC was oxidized to 5caC, and both 5caC and unmethylated cytosine were subsequently converted to uracil through bisulfite-induced deamination, whereas 5hmC was protected from oxidation via 5hmC-specific β-glucosylation [25]. The conversion rates of unmethylated cytosine, 5mCs, and 5hmCs in the bisulfite-/TAB-treated λ-DNA controls were 100%, 99.7%, and 1.5%, respectively (Figure S1). P16H was analyzed using the TAB-MSP.

The proportion of hydroxymethylated S- and AS-strands of the *P16* promoter and exon-1 CGIs were analyzed using DHPLC and clone sequencing, respectively [45,46]. The adjusted ratio of the peak height for the hydroxymethylated region to that of the unmethylated region was used to represent the P16H proportion that was adjusted. The ratio of the P16M peak height to the P16U peak height for *P16*-hemimethylated HCT116 cells was used as a reference. The sequences of the universal primers used to amplify these fragments are listed in Table 1.

Construction of Expression Vectors and Transfection

To construct the *P16*-specific DNA dioxygenase (P16-TET) expression vector, an SP1-like engineered seven-zinc finger protein (7ZFP-6I) [19] that can specifically bind to the 21-bp

fragment (5'-gaggaaggaaacggggcgggg-3', including an Sp1-binding site) within the human *P16* core promoter [24,47], was fused with the catalytic domain (CD: 1418-2136 aa) of human *TET1* (NM_030625.2) [48] and inserted into a pcDNA3.1b vector and then used in transient transfection assays. An inactive P16-TET mutant containing an H1671Y mutation in the CD domain vector was also constructed and used as a negative control vector (Figure S2A). The P16-TET sequence was further integrated into the expression-controllable pTRIPZ vector carrying a "Tet-on" switch (Open Biosystem, USA) (Figure S2B) [19]. Purified P16-TET pTRIPZ plasmid was mixed with VSVG and Δ8.9 (Addgene, USA) to prepare lentivirus transfection particles. The fresh lentivirus particles were used to stably infect AGS and H1299 cells containing homogenously methylated *P16* CpG islands. Doxycycline (Dox; final conc. 0.25 μg/mL) was added to the medium to induce P16-TET expression.

Two *P16*-specific siRNAs (5'-ccgua aaugu ccauu uauatt-3' and 5'–uauaa augga cauuu acggtt-3') were synthesized (GenePharma, Shanghai) and used to transiently transfect cells at a final concentration of 1.0 μg/mL. Two scrambled siRNAs (5'-uucuc cgaac guguc acgutt-3' and 5'-acgug acacg uucgg agaatt-3') were used as negative controls (NC).

Treatment of 5'-Aza-Deoxycytidine (DAC)

The AGS cells were treated with DAC (final concentration 20 nM; Abcam ab120842, Cambridge, UK) for 7 days in the P16-immunostaining assay or 10 days prior to FACS sorting.

Extraction of RNA and Quantitative RT-PCR (qRT-PCR)

Cells were harvested when they reached a confluency of approximately 70%. Total RNA was extracted by TRIzol (Invitrogen, California, USA). The cDNA was reverse-transcribed

using the ImProm-II™ Reverse Transcription System (A3800; Promega). The expression levels of the *ANRIL*, *P16*, *P15*, *P14*, and *TET-1/2/3* genes were analyzed by quantitative RT-PCR using the corresponding primer sets (Table 1), as previously described [20]. Power SYBR Green PCR Master Mix (Fermentas, Canada) was used in the qRT-PCR analyses (ABI-7500FAST). The relative mRNA level was calculated based on the average Ct value of the target gene and the *Alu* reference [$2^{-(Ct_{target\_gene}-Ct_{Alu})}$] [49].

Western Blot and Confocal Microscopy Analysis of the P16 Expression Status

The *P16* mRNA and protein levels in the cells were analyzed as previously described [19]. Rabbit monoclonal antibody against human P16 protein (ab108349, Abcam, Britain) was used in the Western blot assay, and mouse monoclonal antibody against the human P16 protein (Ventana Roche-E6H4, USA) was used in the immunostaining assay.

Cell FACS Sorting

The P16-TET stably transfected H1299 cells (treated with doxycycline for 21 days) and AGS cells (treated with 5-aza-deoxycytidine for 10 days) were fixed with methanol, permeabilized with 0.1% Tween-20 in PBS, pretreated with 10% fetal bovine serum and 0.3 M glycine in PBS, and were then stained with the mouse monoclonal antibody against the human P16 protein (Ventana Roche-E6H4, USA) and the FITC-tagged secondary antibody. The P16-staining cell population proportion was determined using an immuno-fluorescence confocal microscope. These cells were sorted by FACS and divided into three subpopulations, strong-, weak-, and non-P16-staining, using P16-TET H1299 cells without doxycycline treatment or AGS cells without DAC treatment as P16 protein negative controls. According to the confocal analysis results, we setup the cutoff value to sort definite and indefinite P16 protein positive (P16(+) and P16(±)) cell subpopulations. The strong and

weak FITC-staining cells were called as the P16(+) and P16(±) subpopulations, respectively.

IncuCyte ZOOM and Transwell Migration Tests

The long-term live content kinetic imaging platform (IncuCyte Zoom, Essen BioSci, USA) was used to dynamically detect the proliferation and migration of live cancer cells. The phase object confluence (%) was used to generate a cell proliferation curve. The relative wound density, a measure (%) of the density of the wound region relative to the density of the cell region, was used as the metric for cell migration. The transwell migration test was performed as previously described [19].

Xenografts in SCID Mice

Cells stably transfected with the P16-TET vector were induced with 0.25 μg/mL doxycycline for 7 days and then subcutaneously injected into one lower limb of each NOD-SCID mouse (10^5 cells/injection; female, 5 weeks old, 10~20 g, purchased from Beijing Huafukang Biotech). The negative control cells stably transfected with the empty pTRIPZ vector were simultaneously injected into the opposite side of each mouse. These mice were given distilled, sterile water containing 2 μg/mL doxycycline and were sacrificed on the 50^{th} post-transplantation day. The xenografts were weighed and histologically confirmed [19]. Two repeat experiments were performed.

Statistical Analysis

Student's t-test was used for statistical analysis. All *P*-values were two-sided, and a *P*-value of <0.05 was considered to be statistically significant.

ACKNOWLEDGEMENTS

We thank Mr. Jordan M. Grainger (Predoctoral student, Molecular Pharmacology and Experimental Therapeutics, Mayo Clinic, Rochester, Minnesota, USA) and Dr. Huidong Shi (Cancer Center, Georgia Medical College, Augusta, USA) for English language editing.

Ethics approval and consent to participate

The Peking University Cancer Hospital and Institutional Review Boards approved this study. Ethical approval for the animal experiments was obtained.

Disclosure of potential conflicts of interest

The authors have declared that no competing interests exist.

REFERENCES

[1] Tahiliani M, Koh KP, Shen Y, Pastor WA, Bandukwala H, Brudno Y*, et al.* Conversion of 5-methylcytosine to 5-hydroxymethylcytosine in mammalian DNA by MLL partner TET1. Science 2009; 324: 930-935.

[2] Kriaucionis S, Heintz N. The nuclear DNA base 5-hydroxymethylcytosine is present in Purkinje neurons and the brain. Science 2009; 324: 929-930.

[3] He YF, Li BZ, Li Z, Liu P, Wang Y, Tang Q*, et al.* Tet-mediated formation of 5-carboxylcytosine and its excision by TDG in mammalian DNA. Science 2011; 333: 1303-1307.

[4] Ito S, Shen L, Dai Q, Wu SC, Collins LB, Swenberg JA*, et al.* Tet proteins can convert 5-methylcytosine to 5-formylcytosine and 5-carboxylcytosine. Science 2011; 333: 1300-1303.

[5] Gu TP, Guo F, Yang H, Wu HP, Xu GF, Liu W*, et al.* The role of Tet3 DNA dioxygenase in epigenetic reprogramming by oocytes. Nature 2011; 477: 606-610.

[6] Hackett JA, Sengupta R, Zylicz JJ, Murakami K, Lee C, Down TA*, et al.* Germline DNA demethylation dynamics and imprint erasure through 5-hydroxymethylcytosine. Science 2013; 339: 448-452.

[7] Pastor WA, Pape UJ, Huang Y, Henderson HR, Lister R, Ko M*, et al.* Genome-wide mapping of 5-hydroxymethylcytosine in embryonic stem cells. Nature 2011;473:394-7

[8] Ficz G, Branco MR, Seisenberger S, Santos F, Krueger F, Hore TA*, et al.* Dynamic regulation of 5-hydroxymethylcytosine in mouse ES cells and during differentiation. Nature 2011; 473: 398-402.

[9] Yu M, Hon GC, Szulwach KE, Song CX, Zhang L, Kim A*, et al.* Base-resolution analysis of 5-hydroxymethylcytosine in the mammalian genome. Cell 2012; 149: 1368-1380.

[10] Merlo A, Herman JG, Mao L, Lee DJ, Gabrielson E, Burger PC*, et al.* 5' CpG island methylation is associated with transcriptional silencing of the tumor-suppressor p16/cdkn2/mts1 in human cancers. Nature Medicine 1995; 1: 686-692.

[11] Herman JG, Merlo A, Mao L, Lapidus RG, Issa JPJ, Davidson NE*, et al.* Inactivation of the cdkn2/p16/mts1 gene is frequently associated with aberrant dna methylation in all common human cancers. Cancer Research 1995; 55: 4525-4530.

[12] Sun Y, Deng DJ, You WC, Bai H, Zhang L, Zhou J*, et al.* Methylation of p16 CpG islands associated with malignant transformation of gastric dysplasia in a population-based study. Clinical Cancer Research 2004; 10: 5087-5093.

[13] Belinsky SA, Liechty KC, Gentry FD, Wolf HJ, Rogers J, Vu K*, et al.* Promoter hypermethylation of multiple genes in sputum precedes lung cancer incidence in a high-risk cohort. Cancer Res 2006; 66: 3338-3344.

[14] Hall GL, Shaw RJ, Field EA, Rogers SN, Sutton DN, Woolgar JA*, et al.* p16 Promoter

418 methylation is a potential predictor of malignant transformation in oral epithelial
419 dysplasia. Cancer Epidemiol Biomarkers Prev 2008; 17: 2174-2179.
420 [15] Cao J, Zhou J, Gao Y, Gu L, Meng H, Liu H*, et al.* Methylation of p16 CpG Island
421 Associated with Malignant Progression of Oral Epithelial Dysplasia: A Prospective
422 Cohort Study. Clinical Cancer Research 2009; 15: 5178-5183.
423 [16] Jin Z, Cheng Y, Gu W, Zheng Y, Sato F, Mori Y*, et al.* A multicenter, double-blinded
424 validation study of methylation biomarkers for progression prediction in Barrett's
425 esophagus. Cancer Res 2009; 69: 4112-4115.
426 [17] Liu HW, Liu XW, Dong GY, Zhou J, Liu Y, Gao Y*, et al. P16* Methylation as an Early
427 Predictor for Cancer Development From Oral Epithelial Dysplasia: A Double-blind
428 Multicentre Prospective Study. EBioMedicine 2015; 2: 432-437.
429 [18] Gao H-e, Zhang Y, Zhou J, Li Z, Ma J-l, Liu W-d*, et al.* Association between
430 p16 methylation and malignant transformation of gastric dysplasia. Chinese Journal of
431 Cancer Prevention and Treatment 2017; 24: 431-436.
432 [19] Cui C, Gan Y, Gu L, Wilson J, Liu Z, Zhang B*, et al.* P16-specific DNA methylation by
433 engineered zinc finger methyltransferase inactivates gene transcription and promotes
434 cancer metastasis. Genome Biology 2015; 16: 252.
435 [20] Gan Y, Ma W, Wang X, Qiao J, Zhang B, Cui C*, et al.* Coordinate Transcription of
436 A*NRIL* and P*16*Genes Silenced by DNA Methylation. Chinese Journal of Cancer
437 Research 2018; 30: 93-103.
438 [21] Qin SS, Li Q, Zhou J, Liu ZJ, Su N, Wilson J*, et al.* Homeostatic Maintenance of
439 Allele-Specific p16 Methylation in Cancer Cells Accompanied by Dynamic Focal
440 Methylation and Hydroxymethylation. Plos One 2014; 9: E97785.

441 [22] Qin S, Zhang B, Tian W, Gu L, Lu Z, Deng D. Kaiso mainly locates in the nucleus in vivo
442 and binds to methylated, but not hydroxymethylated DNA. Chinese Journal of Cancer
443 Research 2015; 27: 148-155.
444 [23] Liu HW, Liu ZJ, Liu XW, Xu S, Wang L, Liu Y, *et al*. A similar effect of *P16*
445 hydroxymethylation and true-methylation on the prediction of malignant transformation
446 of oral epithelial dysplasia: observation from a prospective study. BMC Cancer 2018;
447 18:918.
448 [24] Zhang B, Xiang S, Zhong Q, Yin Y, Gu L, Deng D. The p16-Specific Reactivation and
449 Inhibition of Cell Migration Through Demethylation of CpG Islands by Engineered
450 Transcription Factors. Human Gene Therapy 2012; 23: 1071-1081.
451 [25] Sun Z, Terragni J, Jolyon T, Borgaro JG, Liu Y, Yu L*, et al.* High-resolution enzymatic
452 mapping of genomic 5-hydroxymethylcytosine in mouse embryonic stem cells. Cell
453 Rep 2013; 3: 567-576.
454 [26] Wang T, Wu H, Li Y, Szulwach KE, Lin L, Li X*, et al.* Subtelomeric hotspots of
455 aberrant 5-hydroxymethylcytosine-mediated epigenetic modifications during
456 reprogramming to pluripotency. Nat Cell Biol 2013; 15: 700-711.
457 [27] Kim M, Park YK, Kang TW, Lee SH, Rhee YH, Park JL*, et al.* Dynamic changes in
458 DNA methylation and hydroxymethylation when hES cells undergo differentiation
459 toward a neuronal lineage. Hum Mol Genet 2014; 23: 657-667.
460 [28] Wen L, Li X, Yan L, Tan Y, Li R, Zhao Y*, et al.* Whole-genome analysis of
461 5-hydroxymethylcytosine and 5-methylcytosine at base resolution in the human
462 brain. Genome Biol 2014; 15: R49.
463 [29] Chen K, Zhang J, Guo Z, Ma Q, Xu Z, Zhou Y*, et al.* Loss of
464 5-hydroxymethylcytosine is linked to gene body hypermethylation in kidney cancer.
465 Cell Res 2016; 26: 103-118.

[30] Li X, Liu Y, Salz T, Hansen KD, Feinberg A. Whole-genome analysis of the methylome and hydroxymethylome in normal and malignant lung and liver. Genome Res 2016; 26: 1730-1741.

[31] Huang Y, Chavez L, Chang X, Wang X, Pastor WA, Kang J*, et al.* Distinct roles of the methylcytosine oxidases Tet1 and Tet2 in mouse embryonic stem cells. Proc Natl Acad Sci U S A 2014; 111: 1361-1366.

[32] Uribe-Lewis S, Stark R, Carroll T, Dunning MJ, Bachman M, Ito Y*, et al.* 5-hydroxymethylcytosine marks promoters in colon that resist DNA hypermethylation in cancer. Genome Biol 2015; 16: 69.

[33] Verma N, Pan H, Doré LC, Shukla A, Li QV, Pelham-Webb B, *et al*. TET proteins safeguard bivalent promoters from de novo methylation in human embryonic stem cells. Nat Genet 2018; 50: 83-95.

[34] Hashimoto H, Liu Y, Upadhyay AK, Chang Y, Howerton SB, Vertino PM, *et al*. Recognition and potential mechanisms for replication and erasure of cytosine hydroxymethylation. Nucleic Acids Res 2012; 40: 4841-4849.

[35] Liu XS, Wu H, Ji X, Stelzer Y, Wu X, Czauderna S*, et al.* Editing DNA Methylation in the Mammalian Genome. Cell 2016; 167: 233-247.

[36] Kearns NA, Pham H, Tabak B, Genga RM, Silverstein NJ, Garber M*, et al.* Functional annotation of native enhancers with a Cas9-histone demethylase fusion. Nat Methods 2015; 12: 401-403.

[37] Lei Y, Zhang X, Su J, Jeong M, Gundry MC, Huang YH*, et al.* Targeted DNA methylation in vivo using an engineered dCas9-MQ1 fusion protein. Nat Commun 2017; 8: 16026.

[38] Konermann S, Brigham MD, Trevino A, Hsu PD, Heidenreich M, Cong L*, et al.* Optical

control of mammalian endogenous transcription and epigenetic states. Nature 2013; 500: 472-476.

[39] Maeder ML, Angstman JF, Richardson ME, Linder SJ, Cascio VM, Tsai SQ*, et al.* Targeted DNA demethylation and activation of endogenous genes using programmable TALE-TET1 fusion proteins. Nat Biotechnol 2013; 31: 1137-1142.

[40] McDonald JI, Celik H, Rois LE, Fishberger G, Fowler T, Rees R*, et al.* Reprogrammable CRISPR/Cas9-based system for inducing site-specific DNA methylation. Biol Open 2016; 5: 866-874.

[41] Saunderson EA, Stepper P, Gomm JJ, Hoa L, Morgan A, Allen MD*, et al.* Hit-and-run epigenetic editing prevents senescence entry in primary breast cells from healthy donors. Nat Commun 2017; 8: 1450.

[42] Bernstein DL, Le Lay JE, Ruano EG, Kaestner KH. TALE-mediated epigenetic suppression of CDKN2A increases replication in human fibroblasts. J Clin Invest 2015; 125: 1998-2006.

[43] Herman JG, Graff JR, Myöhänen S, Nelkin BD, Baylin SB. Methylation-specific PCR: a novel PCR assay for methylation status of CpG islands. Proc Natl Acad Sci U S A 1996; 93: 9821-9826.

[44] Yu M, Hon GC, Szulwach KE, Song CX, Jin P, Ren B*, et al.* Tet-assisted bisulfite sequencing of 5-hydroxymethylcytosine. Nat Protoc 2012; 7: 2159-2170.

[45] Deng DJ, Deng GR, Smith MF, Zhou J, Xin HJ, Powell SM*, et al.* Simultaneous detection of CpG methylation and single nucleotide polymorphism by denaturing high performance liquid chromatography. Nucleic Acids Research 2002; 30: 13E.

[46] Luo DY, Zhang BZ, Lv LB, Xiang SY, Liu YH, Ji JF*, et al.* Methylation of CpG islands of

p16 associated with progression of primary gastric carcinomas. Laboratory Investigation 2006; 86: 591-598.

[47] Zhang B, Xiang S, Yin Y, Gu L, Deng D. C-terminal in Sp1-like artificial zinc-finger proteins plays crucial roles in determining their DNA binding affinity. BMC Biotechnology 2013; 13: 106.

[48] Guo JU, Su Y, Zhong C, Ming GL, Song H. Hydroxylation of 5-methylcytosine by TET1 promotes active DNA demethylation in the adult brain. Cell 2011; 145: 423-434.

[49] Zheng X, Zhou J, Zhang B, Zhang J, Wilson J, Gu L*, et al.* Critical evaluation of Cbx7 downregulation in primary colon carcinomas and its clinical significance in Chinese patients. BMC cancer 2015; 15: 1172.

FIGURE LEGENDS

Figure 1. TAB-DHPLC and TAB sequencing detected 5hmCs in the sense- and antisense-strands of *P16* promoter and exon-1 of HCT116 cells. (***A***-***D***) Results of four amplicons in the sense- and antisense-strands of the *P16* promoter and exon-1 regions are illustrated in the middle chart; Left charts: chromatograms of bisulfite- and TAB-PCR products for four strands. P16M Ctrl and P16U Ctrl: the corresponding PCR products of *P16*-methylated RKO cells and *P16*-unmethylated MGC803 cells; Right images: Results of clone sequencing of HCT116_TAB PCR products for four strands. 5hmC density: 82.9% (290/350) and 17.6% (58/330) for wildtype exon-1 antisense- and sense-strand clones, and 2.0% (5/250) and 22.3% (58/260) for promoter antisense- and sense-strand clones. Each line represents one clone, respectively. Each red dot represents one 5hmC. Green dots indicate TAB-unmodified cytosines. The locations of G-insertion and G-deletion in exon-1 are also labeled. The amplicon sequences of four strands are placed at the top of the

images. M:U and H:N, ratios of the peak height for Methylated-*P16* to Unmethylated-*P16* alleles and Hydroxymethylated-*P16* to Not hydroxymethylated-*P16* alleles in bisulfite-DHPLC and TAB-DHPLC analyses, respectively.

Figure 2. Reactivation of methylated *P16* alleles in H1299 cells 6 days after P16-TET transient transfection. (**A**) qRT-PCR. (**B**) Immunofluorescence staining.

Figure 3. P16-TET induces hydroxymethylation of *P16* CpG islands and reactivates expression of methylated *P16* alleles in H1299 cells. (**A**) TAB-MSP analysis for detecting hydroxymethylated (H)- and nonhydroxymethylated (N)-*P16* CpG alleles in H1299 cells stably transfected with P16-TET or empty control vector after doxycycline treatment. The MSP analysis results were also listed. Genomic DNA from RKO and BGC832 cells was used as P16M and P16U controls in the MSP assays, respectively. (**B**) Western blot analysis for detecting the P16 protein; Dox (+/-): with or without the doxycycline treatment (final conc. 0.25 μg/mL). Proteins from BGC832 cells were used as a P16U/active control. (**C**) qRT-PCR results for detecting *P16* mRNA levels relative to *Alu* RNA levels; (**D**) Immunofluorescence confocal analysis for detecting P16 expression.

Figure 4. P16-TET induces hydroxymethylation of *P16* CpG islands and reactivates expression of methylated-*P16* alleles in AGS cells. (**A**) Bisulfite-DHPLC analysis for detecting methylated-*P16* (P16M) and unmethylated-*P16* (P16U) PCR products for the exon-1 antisense strand in P16-TET-transfected AGS cells with different doxycycline induction times. (**B**) The TAB-DHPLC analysis detected the hydroxymethylated *P16* (P16H) PCR products and nonhydroxymethylated *P16* (P16N) PCR products. (**C** and **D**) Bisulfite and TAB sequencing for detecting 5mC and 5hmC sites, respectively, in the same PCR

products as were analyzed by DHPLC. (**E** and **F**) The results of RT-PCR and Western blot analysis for detecting P16 reactivation in AGS cells.

Figure 5. Characterization of P16H in FACS-sorted subpopulations of H1299 cells with various levels of of *P16* expression reactivation. (**A**) FACS sorting of P16-TET stably transfected H1299 cells with and without Dox treatment. The confocal images of the P16 protein staining status are also attached. (**B**) Detection of the DNA hydroxymethylation status of *P16* alleles in various FACS-sorted H1299 subpopulations with strong, weak, and no P16 immunostaining (P16(+)/(±)/(-)) in the TAB-MSP analysis. (**C**) The results of TAB sequencing for the *P16* CpG islands in the P16-negative subpopulation.

Figure 6. Characterization of P16H in FACS-sorted subpopulations of AGS cells with various levels of *P16* expression reactivation. (**A**) FACS-sorting of P16-TET stably transfected AGS cells with and without DAC treatment. The confocal images of the P16 protein staining status are also attached. (**B**) Detection of the DNA hydroxymethylation status of *P16* alleles in various FACS sorted AGS subpopulations with strong, weak, and no P16-immunostaining (P16(+)/(±)/(-)) in the TAB-MSP analysis. (**C**) The results of TAB-DHPLC for the *P16* CpG islands in three subpopulations. (**D**) The results of TAB sequencing for the antisense strand of *P16* exon-1 in P16(+) and P16(-) subpopulations.

Figure 7. Effects of P16H on the proliferation of H1299 cells *in vitro* and *in vivo*. (***A***) Cell proliferation curves for H1299 cells with and without P16-TET expression in a live content kinetic imaging platform; (**B**) Comparison of weights of H1299 tumor xenografts with and without stable P16-TET transfection in SCID mice; (**C** and **D**) Images of xenografts on the 50^{th} experimental day.

SUPPORTING FIGURE LEGENDS

Figure S1. Characterization of the true methylation and hydroxymethylation states of CpG sites in the *M.sss*I-methylated and 5hmC-containing λ-DNA controls (5mC-ctrl and 5hmC-ctrl). Bisulfite-modified DNA templates were used to discriminate 5mC or 5hmC from unmethylated cytosine. TAB-modified DNA templates were used to discriminate 5hmC from 5mC and unmethylated cytosine. The CpG sites within the consensus sequences are listed above the corresponding clone sequences. The number of 5hmC and 5mC sites within each clone is also listed on the right side. The control DNA was added into the test samples to monitor the conversion status of 5mC, 5hmC, and unmethylated cytosine in genomic DNA by bisulfite and TAB treatments.

Figure S2. Construction of P16-TET expression vector. (**A**) Fragment sequences of the catalytic domain (CD) of the human *TET1* gene were used to construct the wild-type P16-TET and its inactive H1671Y-mutant control. (**B**) The pTRIPZ vector integrated with 7ZFP-6I and the TET1 CD domain.

Figure S3. The demethylation status of *P16* CpG islands and reactivation of *P16* expression in H1299 cells. (**A**) Bisulfite-DHPLC analysis for detecting methylated- and demethylated-*P16* (P16-M and P16-U) in H1299 cells stably transfected with P16-TET or empty control vector after doxycycline treatment for different days; genomic DNA from HCT116 cells was used as a P16-M and P16-U control. (**B**) Bisulfite sequencing analysis for detecting the methylation status of *P16* exon-1 antisense strands from H1299 cells stably transfected with P16-TET and doxycycline-treated for 0, 14, and 28 days.

Figure S4. Effect of P16-TET on transcription of *P16*, *ANRIL*, *P15*, and *P14* genes in the 9p21 locus of H1299 cells stably transfected with the P16-TET pTRIPZ vector and treated with doxycycline for 14 days.

Figure S5. P16 expression status of *P16*-methylated AGS cells stably transfected with P16-TET (or control vector) as shown by in immunostaining. P16-TET cells were cotreated with 5-aza-deoxycytidine (DAC, final concentration 20 nM) or its reagent control for 10 days (without doxycycline treatment). The proportion of P16(+) cells in the confocal microscopy images for each group was automatically counted using the ImageXpress Micro High Content Screening System (Molecular Devices, USA).

Figure S6. Effects of P16-H on the growth of xenograft tumors from H1299 and A549 cells in NOD-SCID mice. (**A**) Images of xenograft tumors from H1299 cells with and without stable P16-TET transfection on the 36th experimental day. (**B**) Images of xenograft tumors from *ink4a/b*-deleted A549 cells with and without stable P16-TET transfection on the 33rd experimental day. The H.E. staining images are also displayed.

Figure S7. Effects of *P16* expression changes induced by P16-TET and *P16* siRNA on the migration of H1299 cells stably transfected with P16-TET *in vitro*. (**A**) IncuCyte ZOOM scratch assay for detecting cell migration. (**B**) Transwell migration assay for detecting the migration of cells with 24 hr incubation. The average cell number (confluence) and s.d. value are displayed in the left charts. (**C**) Rescue assay for detecting the effect of siRNA-knockdown of *P16* expression on the migration of H1299 cells stably transfected with P16-TET and treated with doxycycline for 14 days. The cells (4.5×10^4) transiently transfected with two types of *P16*-specific siRNAs were seeded into each well and

623 incubated for 72 hrs. The expression status of the P16 protein was monitored using
624 Western blot assay.
625

626 ## TABLE

627 **Table 1**. Sequences of oligonucleotides used as primers in various PCR-based assays

Gene name	Entrez gene ID	Assay	Oligo name	Primer sequence (5'→3')	Product size (bp)	PCR Tm (°C)
P16	1029	qRT-PCR	P16-F	gctgcccaacgcaccgaata	180	58
			P16-R	accaccagcgtgtccaggaa		
		DHPLC/Seq	P16-E1F	tttttagaggatttgagggatagg	392	57
			P16-E1R	ctacctaattccaattcccctacaaactt		
			P16-E1SF	gttgtagatttttttatttatttggat	369	56
			P16-E1SR	tccccttacctaaaaaaatacc		
			P16-PF	ttggtagttaggaaggttgtat	367	55
			P16-PR	tttagaggatttgagggatagg		
			P16-PSF	gttttttaaatttttttggagggat	402	55
			P16-PSR	ttggtgttatagggaaagtatgg		
		MSP-M/H	P16-MF	ttattagagggtggggcggatcgc	150	62
			P16-MR	gaccccgaaccgcgaccgtaa		
		MSP-U/N	P16-UF	ttattagagggtggggtggattgt	151	62
			P16-UR	caaccccaaaccacaaccataa		
ANRIL	NR_003529	qRT-PCR	E3-E4R	cagcagaaggtgggcagcagat	145	64
			E3-E4F	ttcctcgacagggcaggcaggt		
P15	1030	qRT-PCR	P15-qF	agtcaaccgtttcgggaggcg	168	58
			P15-qR	accaccagcgtgtccaggaag		
P14	1029	qRT-PCR	P14-qF	gccaggggcgcccgccgctg	236	62
			P14-qR	ggcccggtgcagcaccacca		
ALU		qRT-PCR	ALU-qF	gaggctgaggcaggagaatcg		54
			ALU-qR	gtcgcccaggctggagtg		
GAPDH	2597	(q)RT-PCR	GAPDH-F	gaaggtgaaggtcggagt	226	62
			GAPDH-R	gaagatggtgatgggatttc		
λ-DNA	5hmC-ctrl	PCR	5hmC-F	ggagttggtatgtagggtagaaagg	202	55
			5hmC-R	attcactctctcacctactctct		
	5mC-ctrl	PCR	5mC-F	tttgggttatgtaagttgattttatg	296	55
			5mC-R	caccctacttactaaaatttacacc		

628

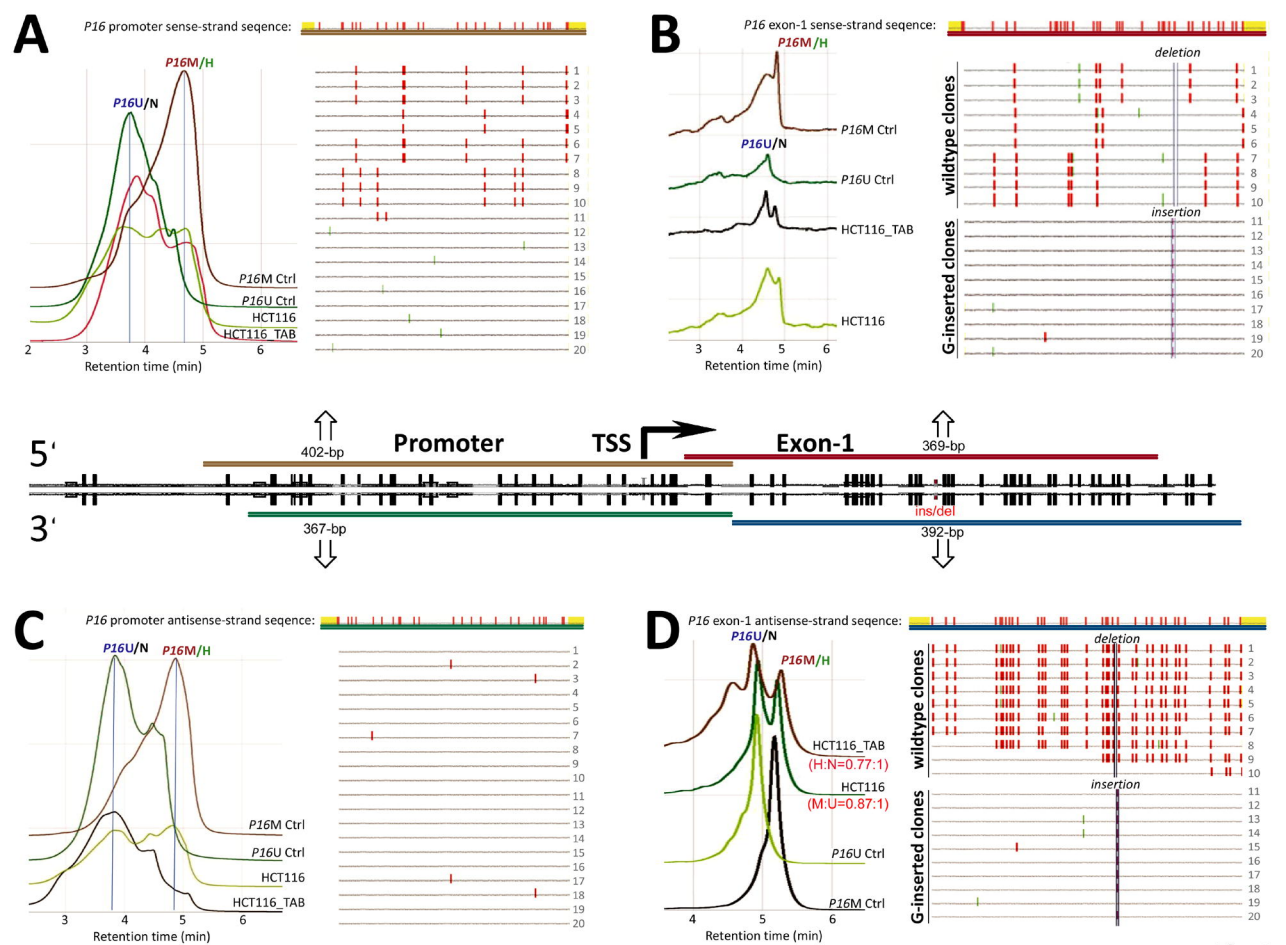
A
P16 promoter sense-strand seqence:
P16M/H
P16U/N
P16M Ctrl
P16U Ctrl
HCT116
HCT116_TAB
Retention time (min)
B
P16 exon-1 sense-strand seqence:
P16M/H
P16U/N
P16M Ctrl
P16U Ctrl
HCT116_TAB
HCT116
Retention time (min)
deletion
wildtype clones
insertion
G-inserted clones
5'
3'
402-bp
Promoter
TSS
Exon-1
369-bp
ins/del
367-bp
392-bp
C
P16 promoter antisense-strand seqence:
P16U/N
P16M/H
P16M Ctrl
P16U Ctrl
HCT116
HCT116_TAB
Retention time (min)
D
P16 exon-1 antisense-strand seqence:
P16U/N
P16M/H
HCT116_TAB
(H:N=0.77:1)
HCT116
(M:U=0.87:1)
P16U Ctrl
P16M Ctrl
Retention time (min)
deletion
wildtype clones
insertion
G-inserted clones

Fig.1

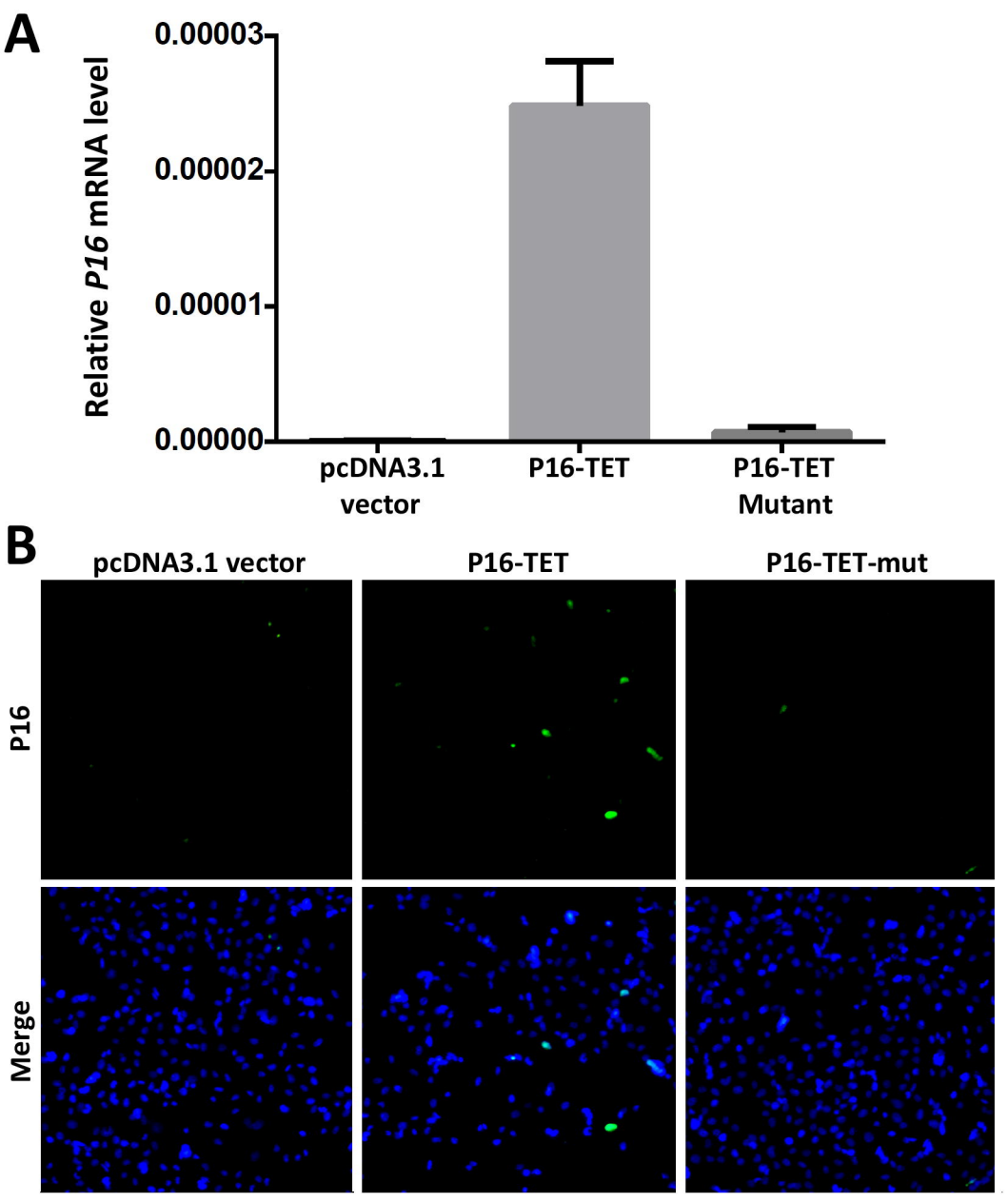
A
Relative P16 mRNA level
0.00003
0.00002
0.00001
0.00000
pcDNA3.1 vector
P16-TET
P16-TET Mutant
B
pcDNA3.1 vector
P16-TET
P16-TET-mut
P16
Merge

Fig.2

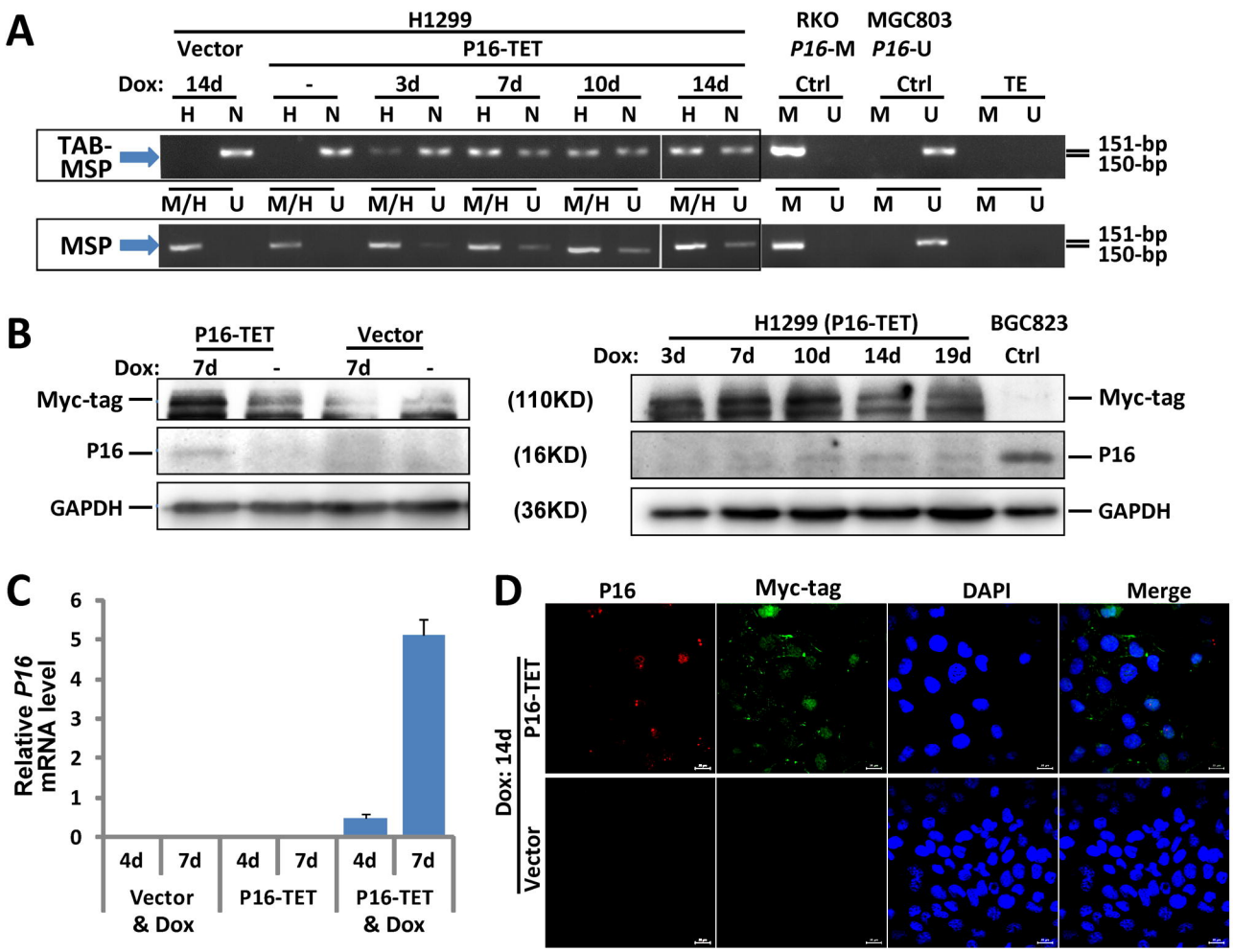
A
H1299
Vector
P16-TET
RKO
P16-M
MGC803
P16-U
Dox: 14d - 3d 7d 10d 14d
Ctrl
Ctrl
TE
H N H N H N H N H N H N
M U M U M U
TAB-MSP
MSP
M/H U
151-bp
150-bp
B
P16-TET
Vector
Dox: 7d - 7d -
Myc-tag
P16
GAPDH
H1299 (P16-TET)
BGC823
Dox: 3d 7d 10d 14d 19d Ctrl
(110KD)
(16KD)
(36KD)
C
Relative P16 mRNA level
0 1 2 3 4 5 6
4d 7d 4d 7d 4d 7d
Vector & Dox
P16-TET
P16-TET & Dox
D
P16
Myc-tag
DAPI
Merge
Dox: 14d
P16-TET
Vector

Fig.3

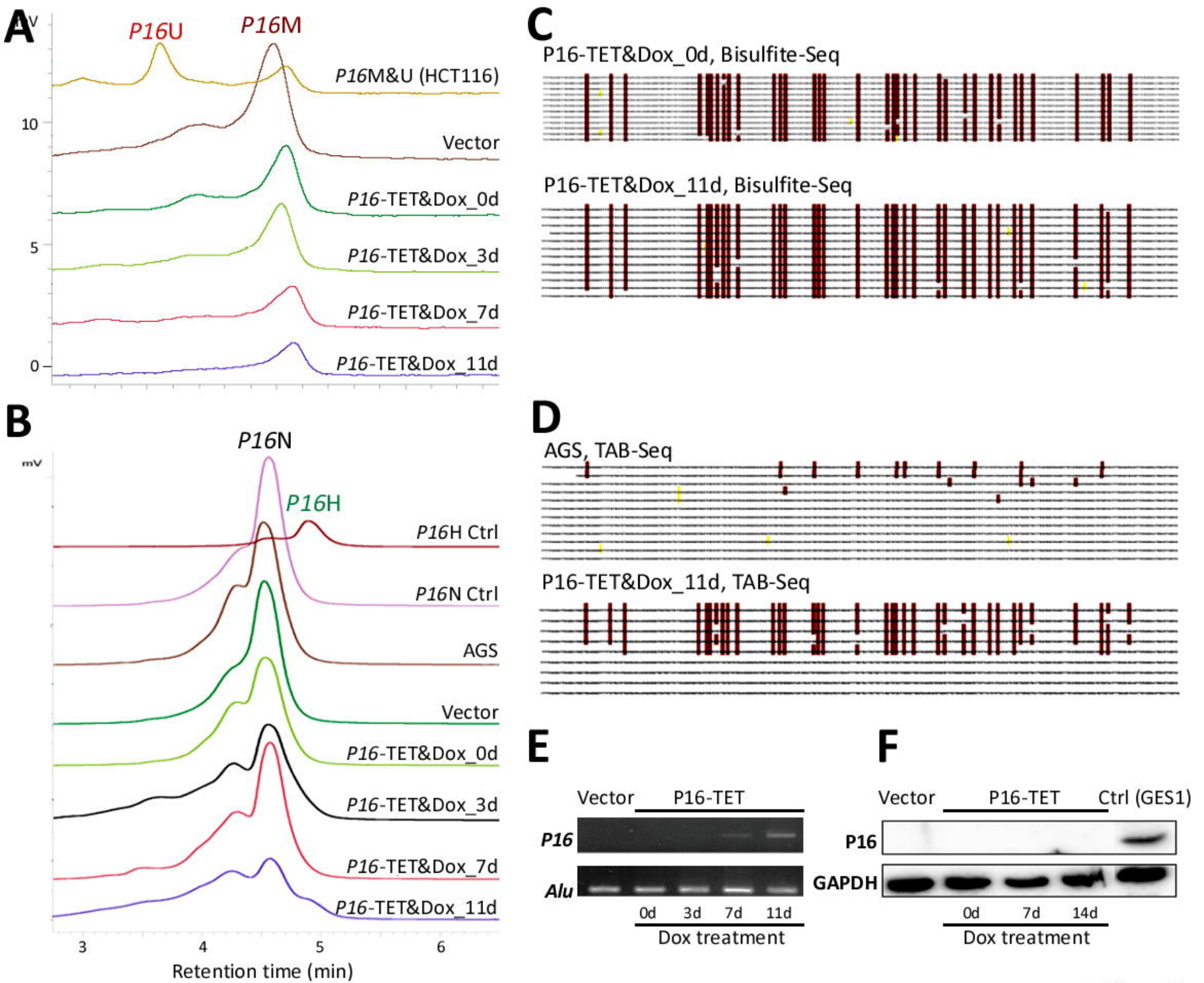
A
P16U
P16M
P16M&U (HCT116)
Vector
P16-TET&Dox_0d
P16-TET&Dox_3d
P16-TET&Dox_7d
P16-TET&Dox_11d
10
5
0
B
P16N
P16H
P16H Ctrl
P16N Ctrl
AGS
Vector
P16-TET&Dox_0d
P16-TET&Dox_3d
P16-TET&Dox_7d
P16-TET&Dox_11d
3
4
5
6
Retention time (min)
C
P16-TET&Dox_0d, Bisulfite-Seq
P16-TET&Dox_11d, Bisulfite-Seq
D
AGS, TAB-Seq
P16-TET&Dox_11d, TAB-Seq
E
Vector
P16-TET
P16
Alu
0d
3d
7d
11d
Dox treatment
F
Vector
P16-TET
Ctrl (GES1)
P16
GAPDH
0d
7d
14d
Dox treatment

Fig.4

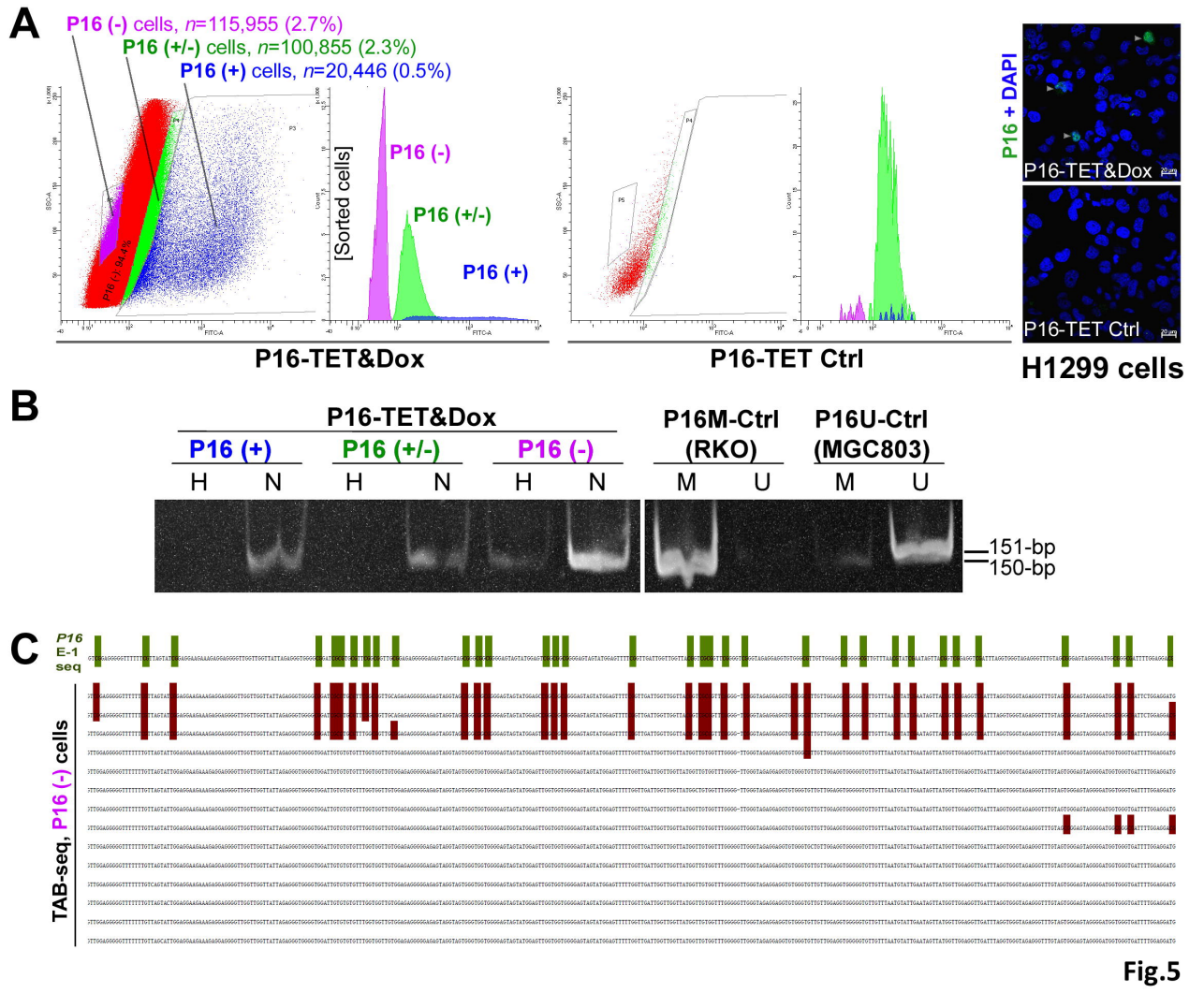
A
P16 (-) cells, n=115,955 (2.7%)
P16 (+/-) cells, n=100,855 (2.3%)
P16 (+) cells, n=20,446 (0.5%)
P16 (-) 94.4%
[Sorted cells]
P16 (-)
P16 (+/-)
P16 (+)
P16-TET&Dox
P16-TET Ctrl
P16 + DAPI
P16-TET&Dox
P16-TET Ctrl
H1299 cells
B
P16-TET&Dox
P16 (+)
P16 (+/-)
P16 (-)
H
N
H
N
H
N
P16M-Ctrl (RKO)
P16U-Ctrl (MGC803)
M
U
M
U
151-bp
150-bp
C
P16 E-1 seq
TAB-seq, P16 (-) cells

Fig.5

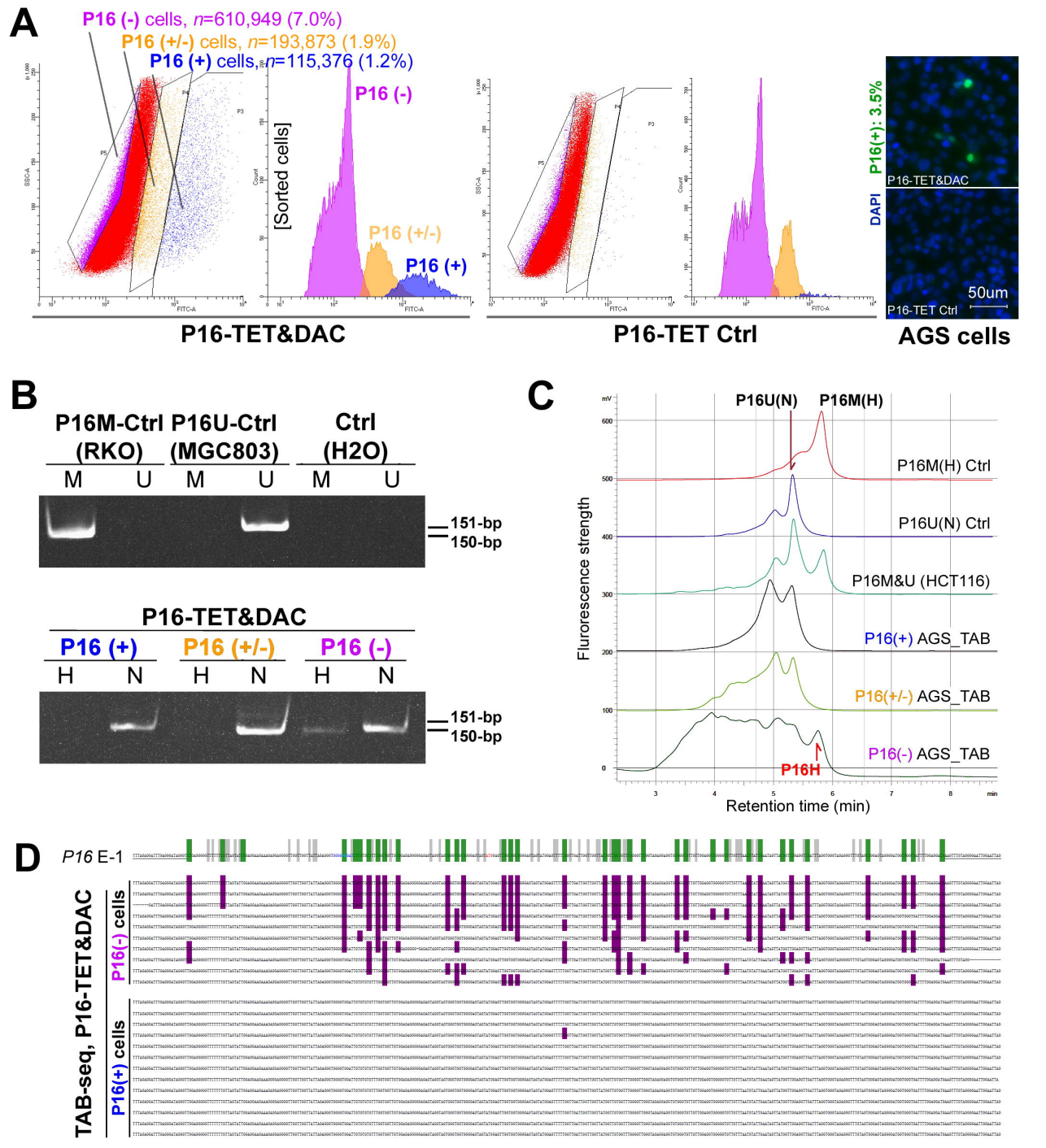
A
P16 (-) cells, n=610,949 (7.0%)
P16 (+/-) cells, n=193,873 (1.9%)
P16 (+) cells, n=115,376 (1.2%)
[Sorted cells]
P16 (-)
P16 (+/-)
P16 (+)
P16-TET&DAC
P16-TET Ctrl
P16(+): 3.5%
DAPI
P16-TET&DAC
P16-TET Ctrl
50um
AGS cells
B
P16M-Ctrl (RKO)
P16U-Ctrl (MGC803)
Ctrl (H2O)
M
U
151-bp
150-bp
P16-TET&DAC
P16 (+)
P16 (+/-)
P16 (-)
H
N
151-bp
150-bp
C
P16U(N)
P16M(H)
P16M(H) Ctrl
P16U(N) Ctrl
P16M&U (HCT116)
P16(+) AGS_TAB
P16(+/-) AGS_TAB
P16(-) AGS_TAB
P16H
Fluorescence strength
Retention time (min)
D
P16 E-1
TAB-seq, P16-TET&DAC
P16(-) cells
P16(+) cells

Fig.6

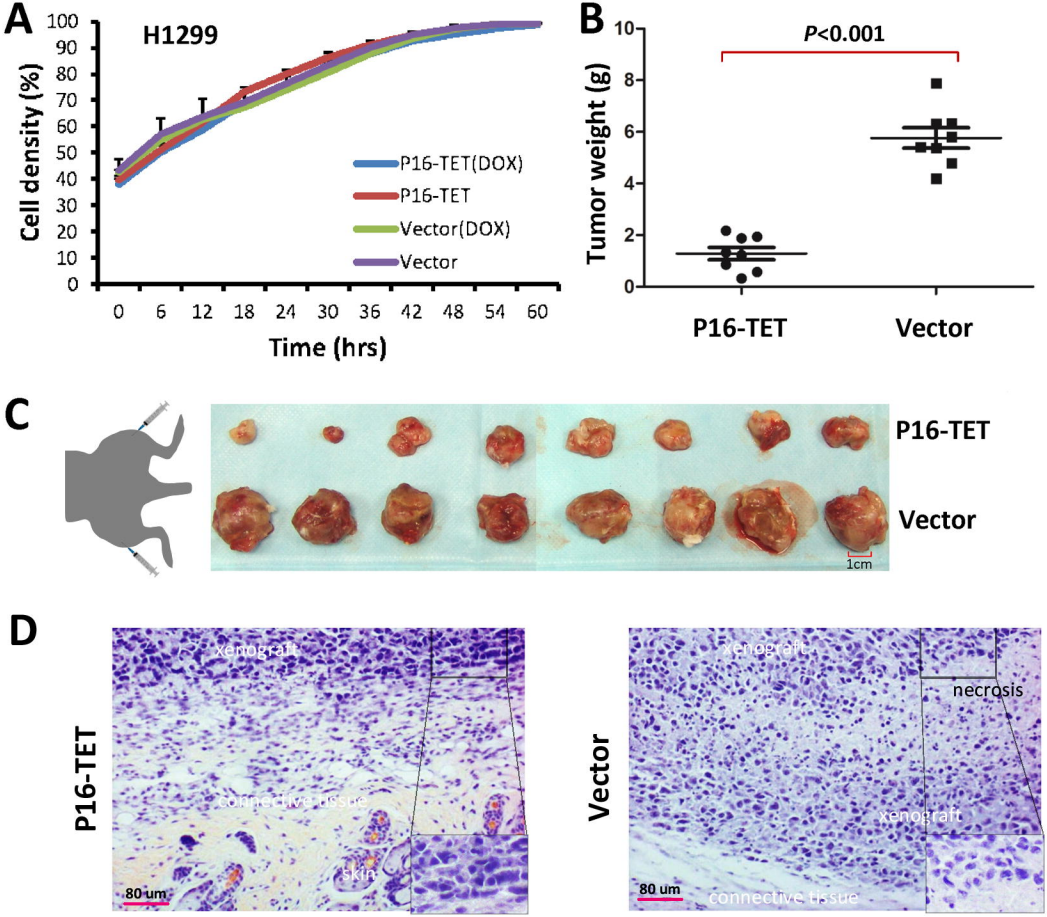
A
H1299
Cell density (%)
Time (hrs)
P16-TET(DOX)
P16-TET
Vector(DOX)
Vector
B
P<0.001
Tumor weight (g)
P16-TET
Vector
C
P16-TET
Vector
1cm
D
P16-TET
xenograft
connective tissue
skin
80 um
Vector
xenograft
necrosis
xenograft
80 um
connective tissue

Fig.7

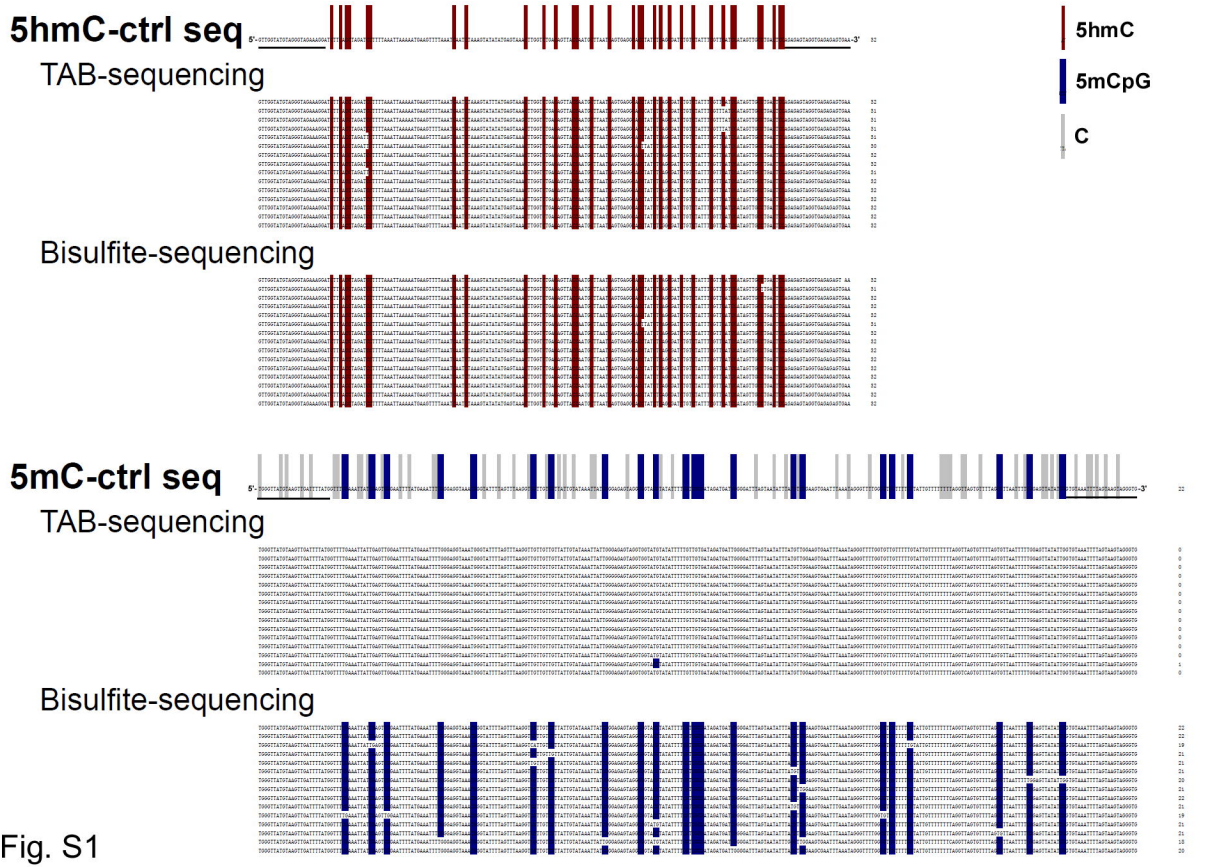
5hmC-ctrl seq
TAB-sequencing
Bisulfite-sequencing
5mC-ctrl seq
TAB-sequencing
Bisulfite-sequencing
5hmC
5mCpG
C

Fig. S1

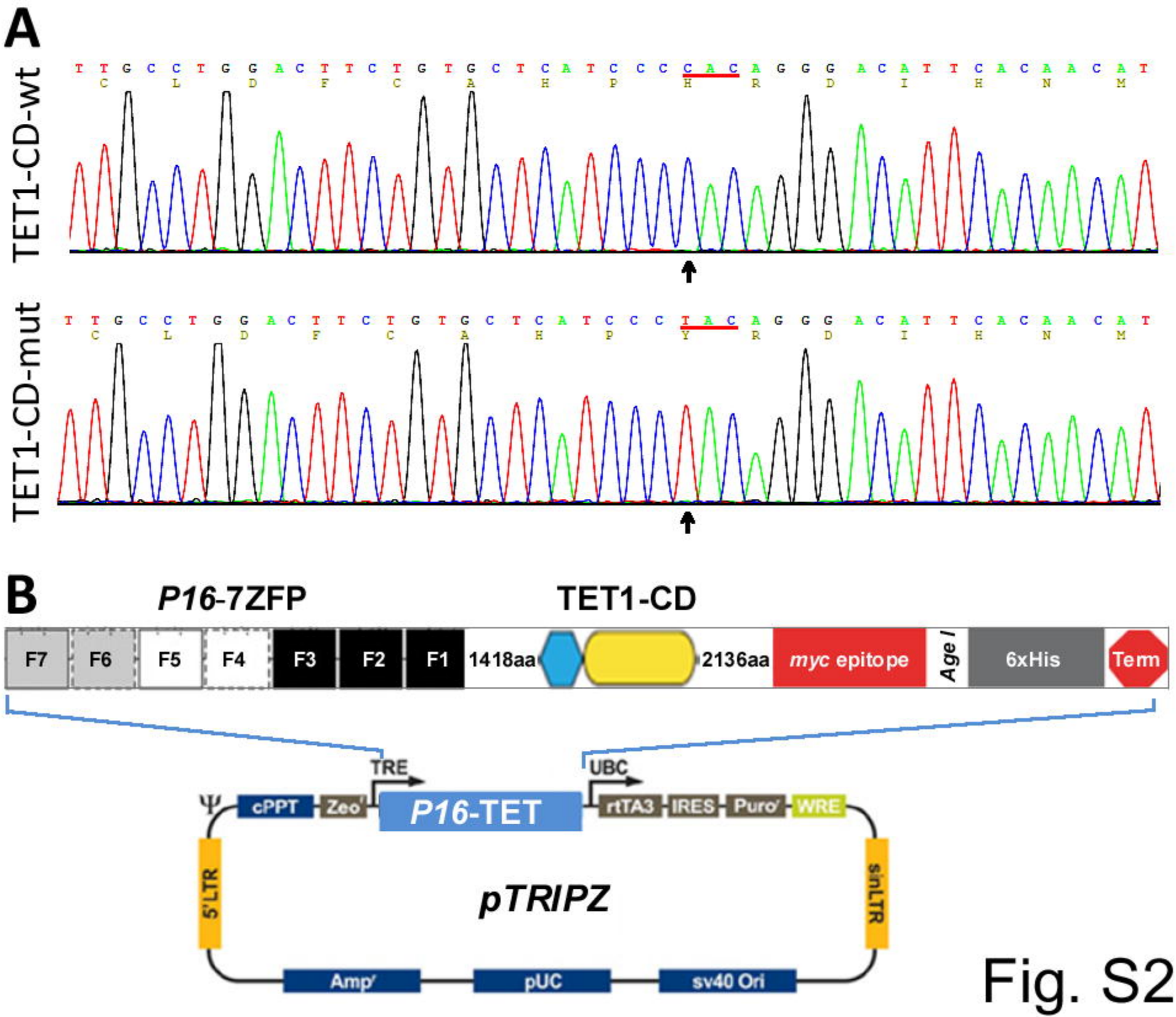
A
TET1-CD-wt
T T G C C T G G A C T T C T G T G C T C A T C C C C A C A G G G A C A T T C A C A A C A T
C L D F C A H P H R D I H N M
TET1-CD-mut
T T G C C T G G A C T T C T G T G C T C A T C C C T A C A G G G A C A T T C A C A A C A T
C L D F C A H P Y R D I H N M
B
P16-7ZFP
TET1-CD
F7
F6
F5
F4
F3
F2
F1
1418aa
2136aa
myc epitope
Age I
6xHis
Term
TRE
UBC
Ψ
cPPT
Zeo'
P16-TET
rtTA3
IRES
Puro'
WRE
5'LTR
pTRIPZ
sinLTR
Amp'
pUC
sv40 Ori

Fig. S2

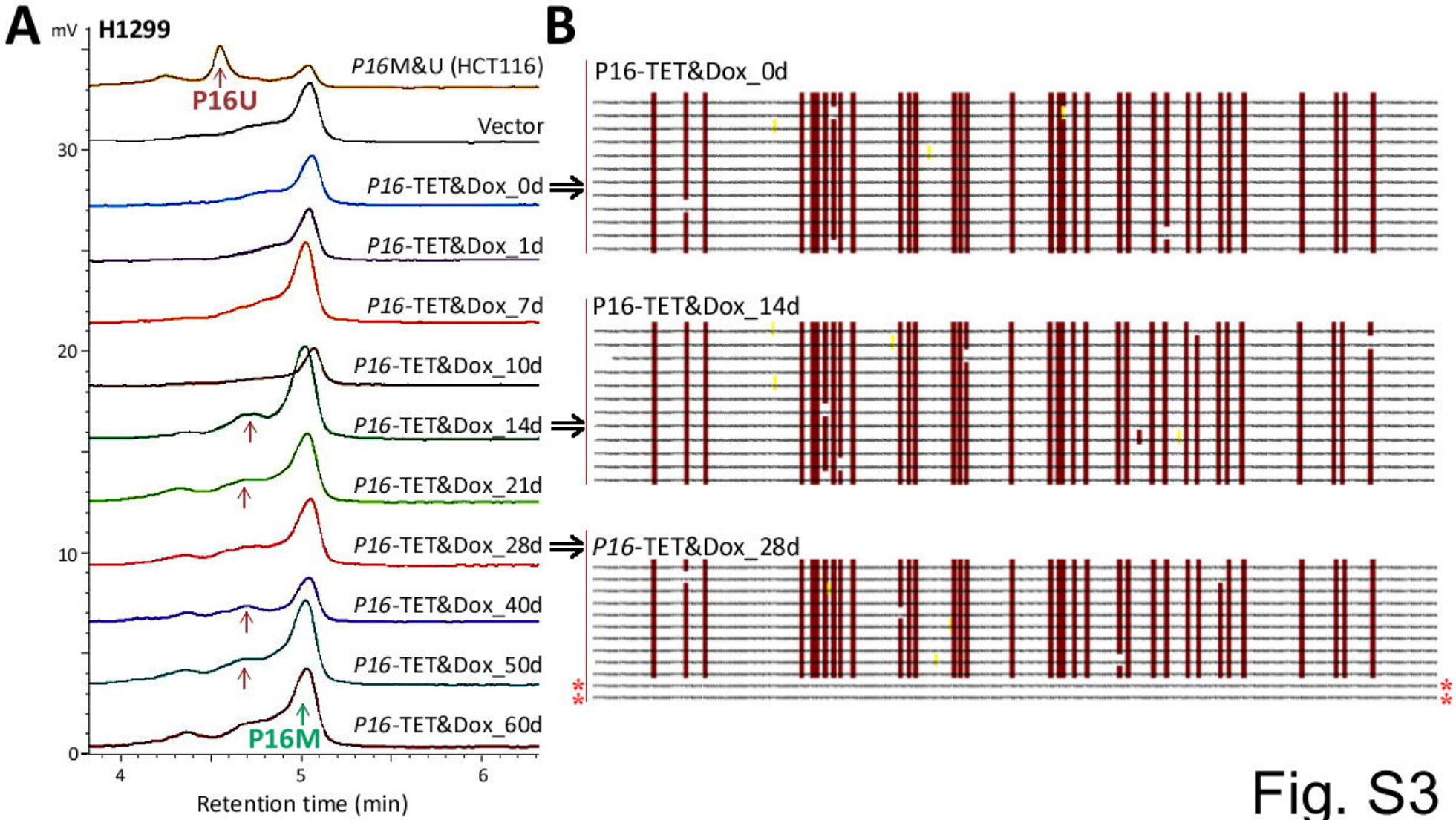
A
mV
H1299
P16M&U (HCT116)
P16U
Vector
P16-TET&Dox_0d
P16-TET&Dox_1d
P16-TET&Dox_7d
P16-TET&Dox_10d
P16-TET&Dox_14d
P16-TET&Dox_21d
P16-TET&Dox_28d
P16-TET&Dox_40d
P16-TET&Dox_50d
P16-TET&Dox_60d
P16M
30
20
10
0
4
5
6
Retention time (min)
B
P16-TET&Dox_0d
P16-TET&Dox_14d
P16-TET&Dox_28d

Fig. S3

Fig. S4

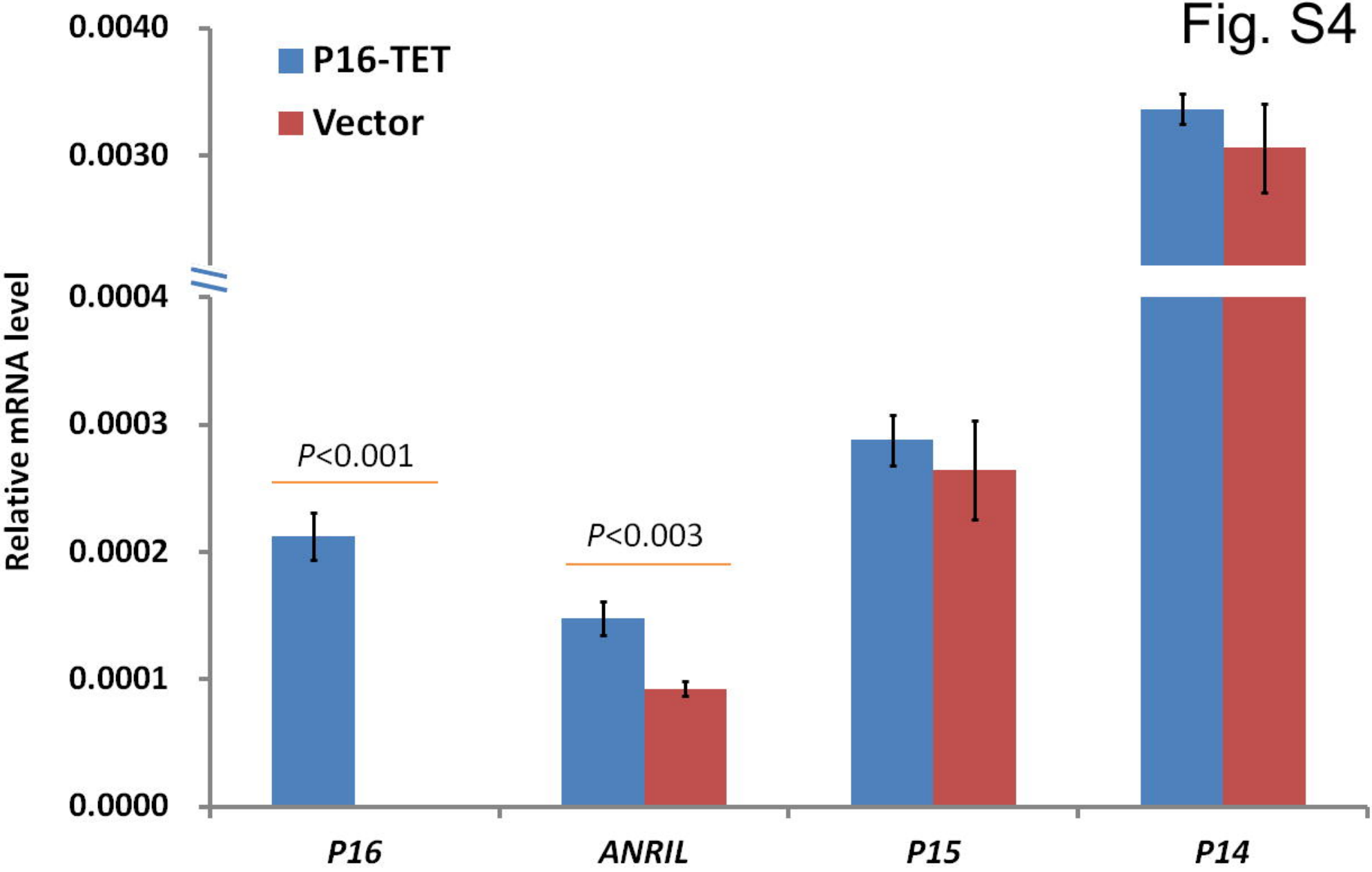
P16-TET
Vector
Relative mRNA level
0.0040
0.0030
0.0004
0.0003
0.0002
0.0001
0.0000
P<0.001
P<0.003
P16
ANRIL
P15
P14

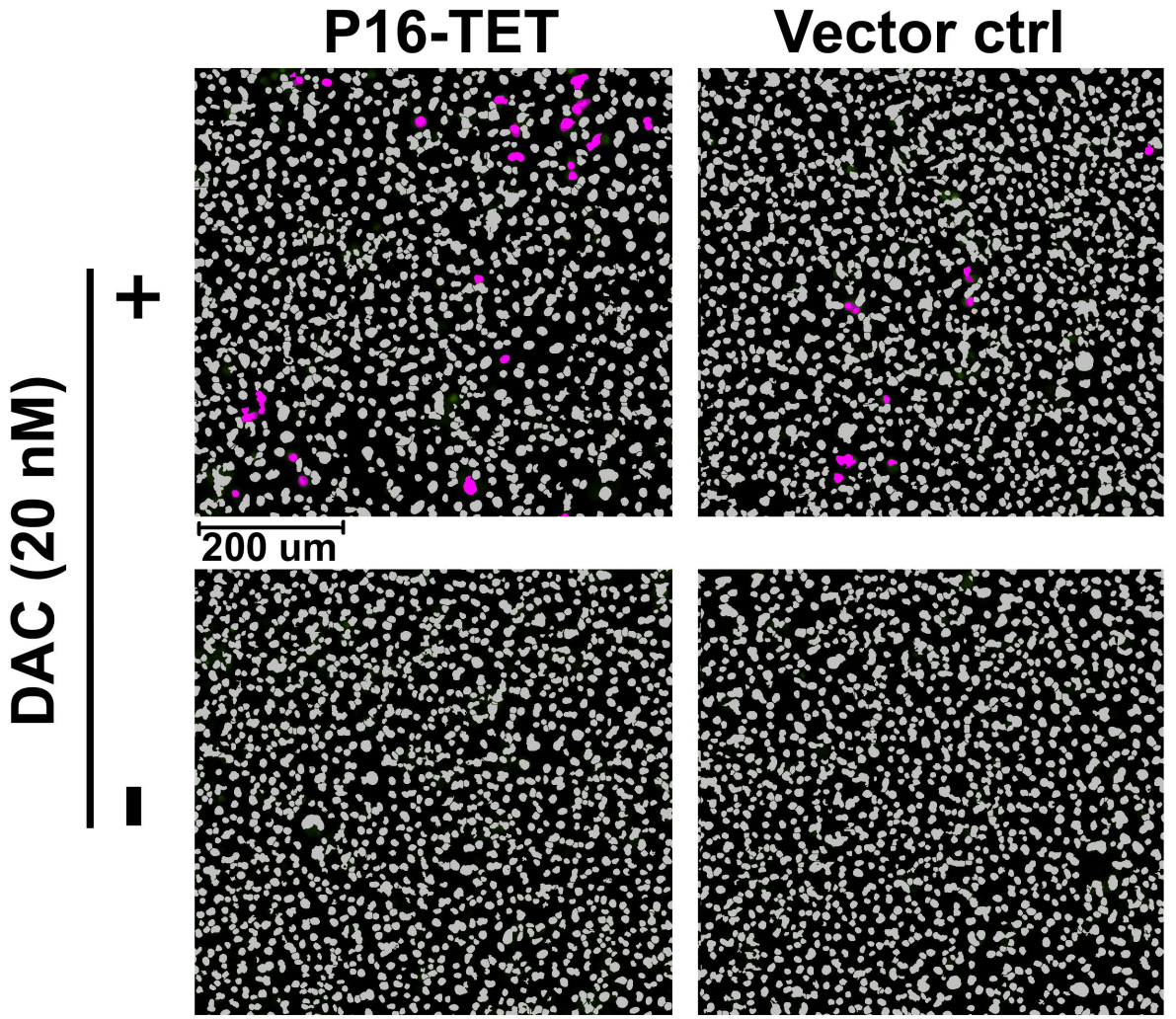
P16-TET
Vector ctrl
DAC (20 nM)
+
-
200 um

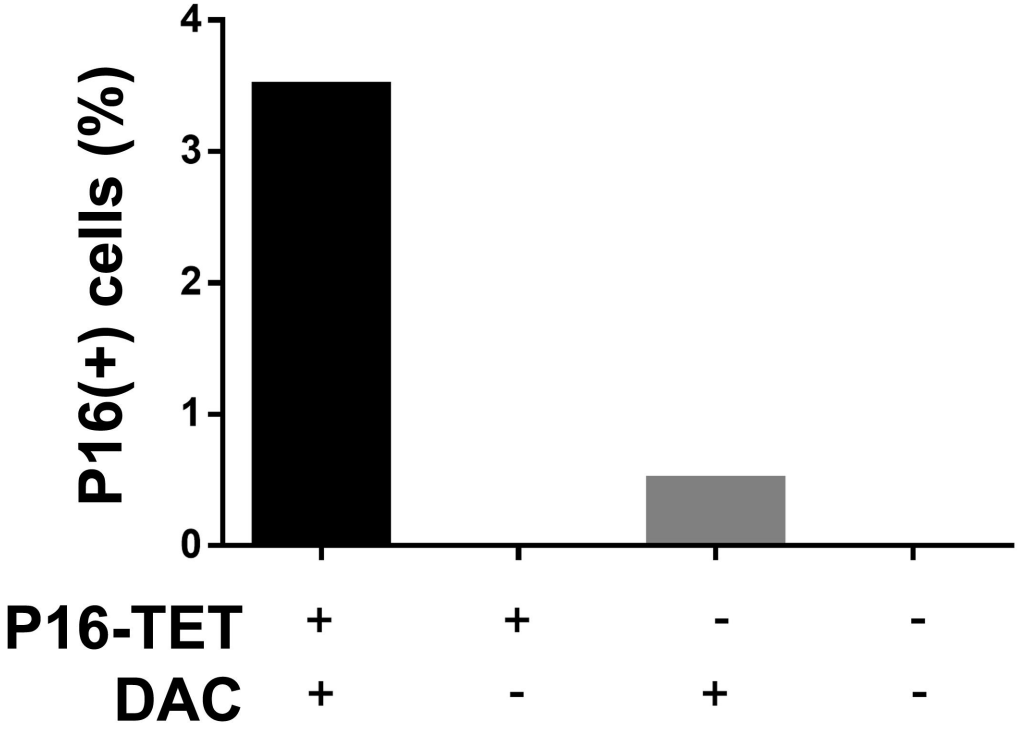
P16(+) cells (%)
4
3
2
1
0
P16-TET + + - -
DAC + - + -

Fig. S5

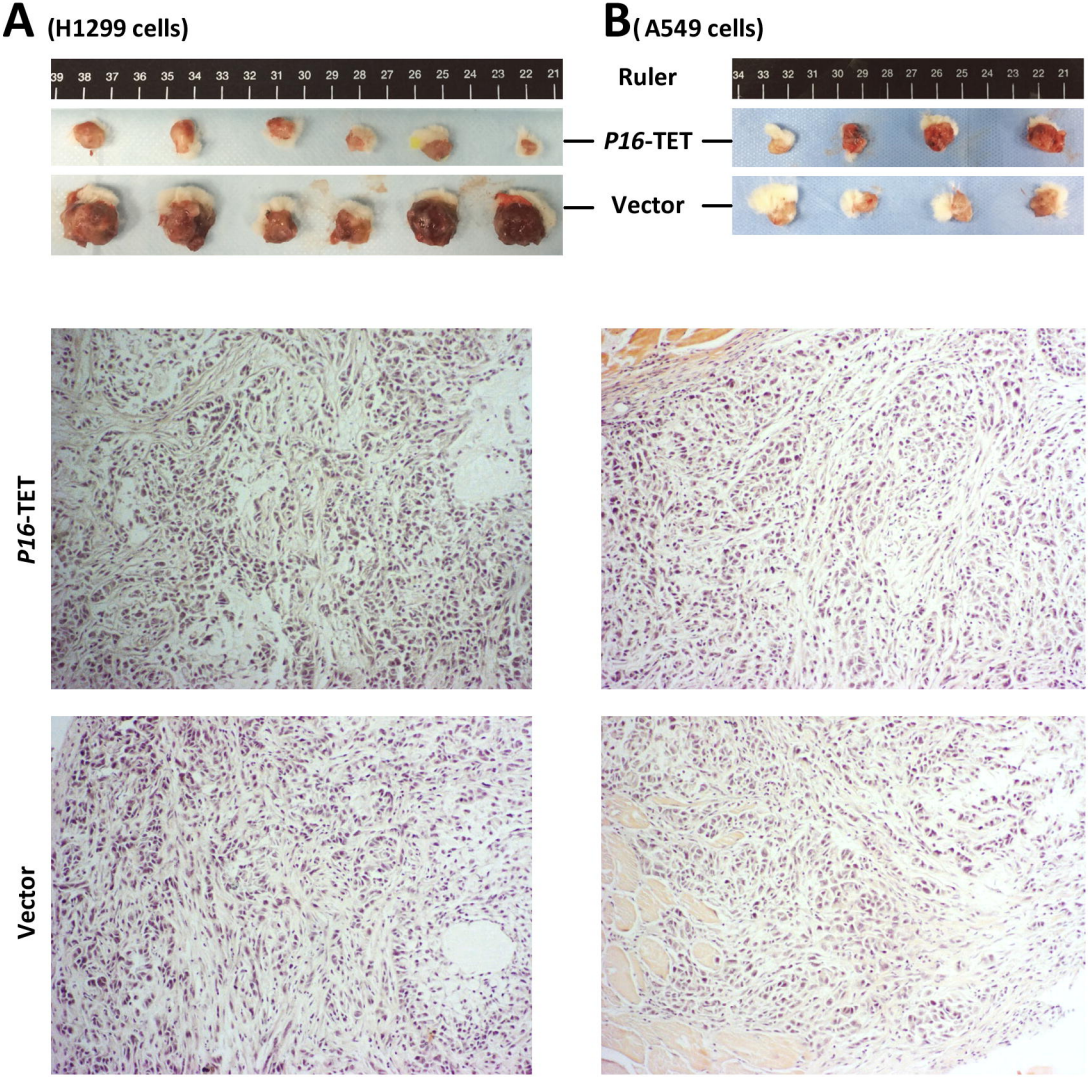
A (H1299 cells)
B (A549 cells)
Ruler
P16-TET
Vector
P16-TET
Vector

Fig. S6

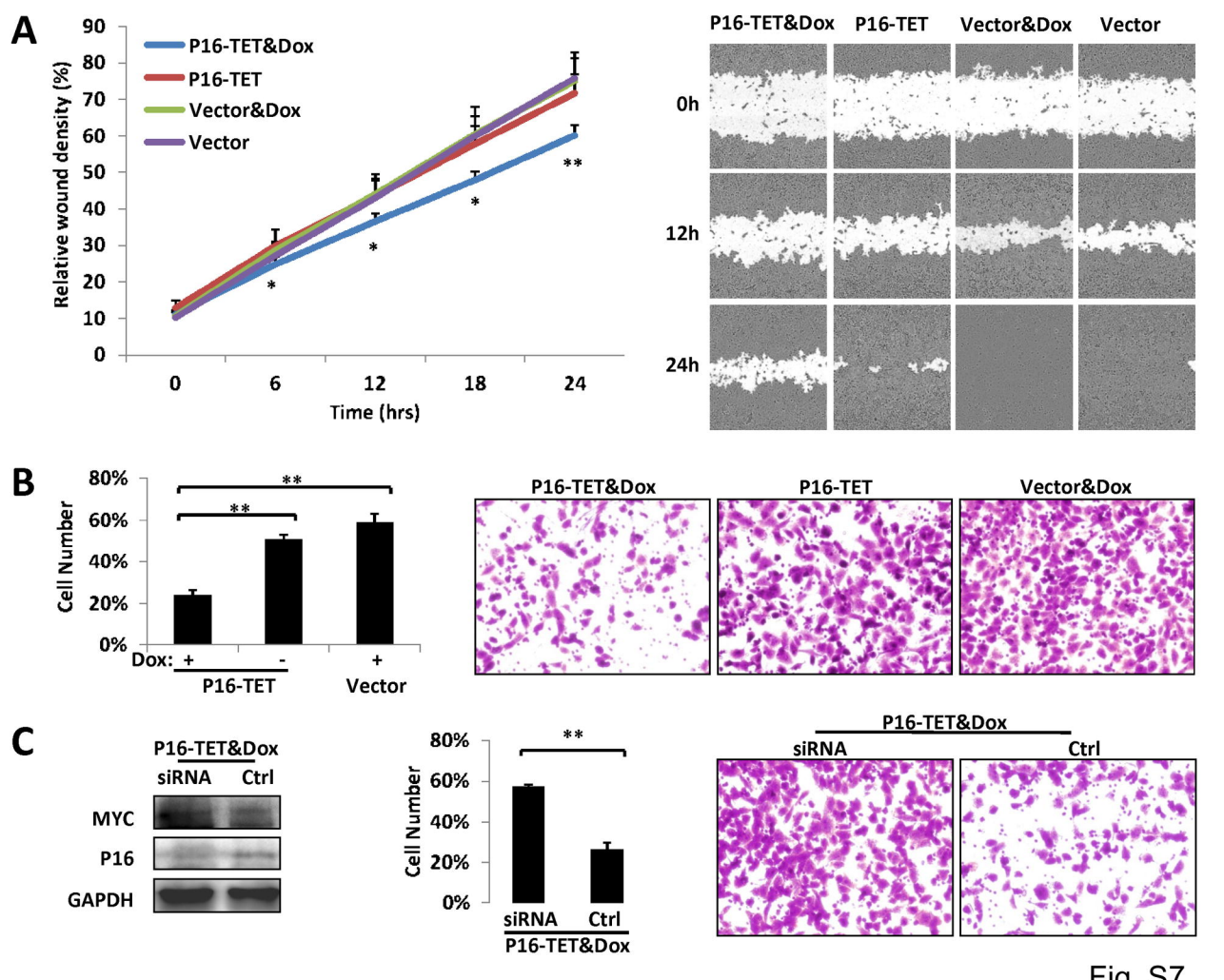
A
P16-TET&Dox
P16-TET
Vector&Dox
Vector
Relative wound density (%)
Time (hrs)
0h
12h
24h
B
Cell Number
Dox: + - +
P16-TET
Vector
C
siRNA
Ctrl
MYC
P16
GAPDH
P16-TET&Dox

Fig. S7